Addis Ababa University

Addis Ababa Institute of Technology

School of Multidisciplinary Engineering

Center for Materials Engineering

Electronic Properties of 2D Vander Waals Heterostructures of Janus Transition Metal Dichalcogenides with WS_2 Monolayer for Photovoltaic Devices: A First Principle Study

A Thesis Submitted to School of Graduate Studies in Partial Fulfillment of the Requirements for the Degree of Master of Science in Materials Engineering

By

Tsigie Getie Adane

June, 2020

Addis Ababa, Ethiopia

Addis Ababa University

School of Graduate Studies

Addis Ababa Institute of Technology

Electronic Properties of 2D Van der Waals Heterostructures of Janus Transition Metal Dichalcogenides with WS_2 Monolayer for Photovoltaic Devices: A First Principle Study

By: Tsigie Getie Adane

A Thesis Submitted to School of Graduate Studies in Partial Fulfillment of the Requirements for the Degree of Master of Science in Materials Engineering

Approved by Board of Examiners

Sintayehu Nibret (Dr)	_____	_____
Advisor	Signature	Date
Georgies Alene (Dr)	_____	_____
Co. Advisor	Signature	Date
Tekalign Debela (Dr)	_____	_____
Co. Advisor	Signature	Date
Yedilfana Setarge (Dr)	_____	_____
External Examiner	Signature	Date
Anteneh Marelign (Dr)	_____	_____
Internal Examiner	Signature	Date

DECLARATION

I, the undersigned, hereby declare that this thesis is my original work, has not been submitted in any previous application for a degree and that all sources of materials used for this thesis have been duly acknowledged.

Name: Tsigie Getie Adane

Signature: _____

Date of submission: June 19, 2020

Abstract

Building two-dimensional (2D) heterostructure emerges novel properties, with promising applications in photovoltaic (PV) cells. By performing density functional theory (DFT) based first-principles calculations, electronic properties of WS_2 and Janus transition-metal dichalcogenides (JTMDs) monolayers were calculated and depending on the lattice mismatch, layered 2D JTMDs/WS_2 heterostructures were formed. The formation of the JTMDs/WS_2 van der Waals (vdW) heterostructures have shown great potential for the design of novel electronic devices. In this study, Janus MoSSe/WS_2, WSSe/WS_2, and MoSTe/WS_2 heterostructures were developed and their structural and electronic properties were evaluated using first principles calculations based on DFT calculations using Quantum ESPRESSO and VASP codes. It was found that the heterostructures bandgap is smaller than the Janus TMDs and WS_2 monolayer. Structural relaxations were performed using generalized-gradient approximation (GGA) approaches for both the monolayers and heterostructures. Structural stability and electronic properties of JTMDs/WS_2 vdW heterostructures with AC and AD stacking were investigated which are the most stable configuration compared with other configurations based on the binding energy and the interlayer distance. Results show that the Janus MoSTe/WS_2, MoSSe/WS_2, and AD-configuration of WSSe/WS_2 vdW heterostructures are indirect bandgap semiconductor, but WSSe/WS_2 with AC-configuration is a direct bandgap. The JTMDs/WS_2 vdW heterostructures exhibited a bandgap in the range of 1.54 to 0.54eV. In addition, MoSSe/WS_2 and MoSTe/WS_2 heterostructures displayed a type-II band alignment which is important to improve the photoelectric conversion efficiency. However, the band alignment of WSSe/WS_2 heterostructure is difficult to identify and need additional calculations. First principles study shows that the investigated 2D heterostructures have a suitable bandgap for photovoltaic applications. Among the JTMDs/WS_2 vdW heterostructures, MoSSe/WS_2 and MoSTe/WS_2 manifest type-II band alignment, making them promising candidates for photovoltaic (PV) applications.

Keywords: JTMDs/WS_2 heterostructures, Type-II band alignment, bandgap, photovoltaic

Acknowledgments

On top of everything, I praise the almighty God for his relentless help to finish and achieve this thesis and master's degree as well.

Foremost, I would like to express my sincere gratitude to my advisors Dr. Georgies Alene and Dr. Sintayehu Nibret for the continuous support and guidance throughout the work of my MSc thesis. Their patience, motivation, enthusiasm, and immense knowledge was very important to my work.

Equivalently, I would like to thank Dr. Tekalign Debela (Research Professor at Department of Nano and Advanced Materials, College of Engineering, Jeonju University, Republic of Korea). For his persistent help and advice given to me during the course of this thesis. It would have been very difficult had he not been involved in my thesis work.

Finally, I would like to thank my family for their support and encouragement. You are always there, not only for this work, but all the time.

Table of Contents

List of Tables

List of Figures

Abbreviations

BZ	Brillouin zone
2D	Two dimensional
JTMD	Janus transitional metal dichalcogenide
DFT	Density Functional Theory
DOS	Density of state
PDOS	partial density of states
TDOS	Total density of state
LDA	Local Density Approximation
GGA	Generalized Gradient Approximation
W	Tungsten
S	sulfur
Mo	Molybdenum
PP	Pseudopotential
Se	Selenium
Te	Tellurium
Ry	Rydberg
eV	Electron volt
Eb	Binding energy
PW	Plane wave
PWscf	Plane wave self consistence field
LDA	Local Density Approximation
Quantum ESPRESSO	Quantum opEn-Source Package for Research in Electronic Structure, Simulation, and Optimization
PBE	Perdew–Burke–Ernzerhof functional
VASP	Vienna Ab-initio Simulation Package
PV	Photovoltaic
vdW	van der Waals
TMDCs	transition metal dichalcogenides
VBM	valence band maximum
CBM	conduction band minimum
CBO	Conduction Band Offset
VBO	Valance Band Offset
LEDs	light-emitting diodes
NIR	near infrared

PWPP	plane wave pseudopotential
Voc	Open circuit voltage
I_{sc}	Short-circuit current
Exc	Exchange correlation functional
EQE	external quantum efficiency
PCE	power conversion efficiency

1 Introduction

1.1 Background

Among Ethiopia's over 112 million populations[1], more than 80% live in rural areas[2]and most of them still have no access to electricity. It is very expensive to reach these areas through grid extension because of the low demand and sparse population distribution. Therefore, to meet the electricity demands of the rural populations off grid technology is an ideal choice. The increase in the emission of pollutants and greenhouse gases into the environment, depletion of world petroleum reserves**,** instability of world political condition, and economic considerations stimulates the need to use renewable energy source for the off-grid technology. Among the renewable energy technology, solar cell technology is growing very fast in the past decades and the price is dropping amazingly. Even the photovoltaic technology energy sources are already in grid party in some parts of the world. Photovoltaic device is an important off-grid power source since it uses inexhaustible solar energy, has a rapid response, can operate at moderate temperatures, and produces no pollution while producing electricity and conventional energy sources, such as fossil fuels, are becoming depleted, thus demanding fast and steady implementation of renewable energy.

The solar photovoltaic (PV) energy conversion contributes significantly to our total renewable energy resources and is primarily dependent on Si-based p–n homojunction solar cells. However, these solar cells are not cost effective, and their efficiency is restricted by the Shockley–Queisser limit [3]. The main factors that limit to achieve the maximum efficiency in silicon homojunction solar cells are spectral loss, optical loss and electrical losses. More recently, 2D (two-dimensional) nanomaterials have shown promise for the development of cost-effective and efficient PV devices through integration with conventional bulk semiconductors due to their unique optical , electronic and mechanical properties[4].

Technology is based on the understanding of the material systems. Depending on the application, specified material properties are required. With 2D materials, the thickness of the material may also be reduced down to a single atom. This is the case with the most well-known 2D material-graphene and is where the most interesting property changes take placed 2D materials have been

attracting increasing attention due to the many novel properties originating from the bulk to monolayer transition.

Graphene was the first 'new' isolated 2D material in 2004[5]. Afterwards, hundreds of other 2D materials with a wide range of properties were studied as shown in Figure 1. Among the 2D family, transition metal dichalcogenides (TMDCs)have been most widely studied; MoS_2 as the representative TMDC material, its electrical, optical as well as other physical properties[6],[7],[8].

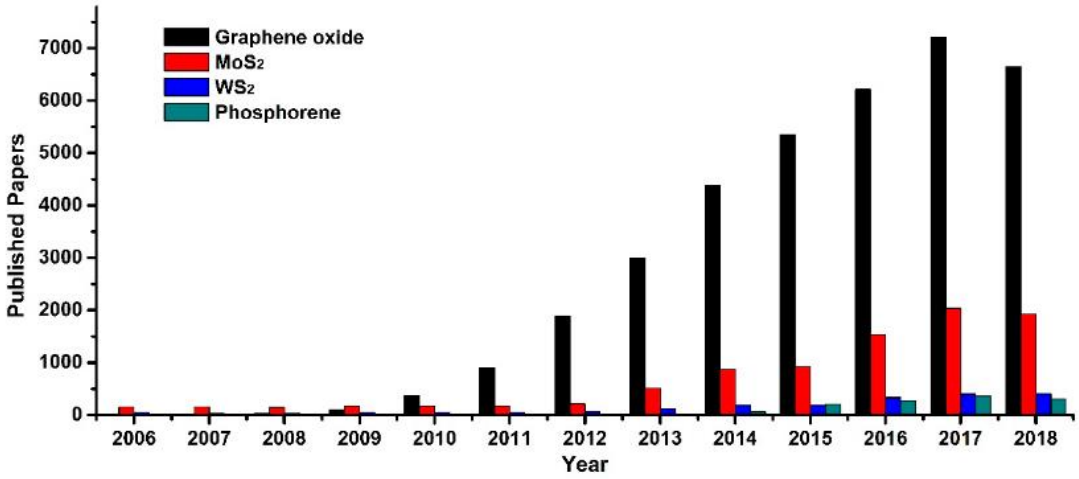

Figure 1**.** Number of published papers vs. year of publication for “graphene oxide”, “MoS2”, “WS2” and “phosphorene” or “exfoliated black phosphorus”[9]

TMDCs are a layered material, which are formed by combining the transition metals (M = Mo, W, Pt, Ti, Hf, Ta) with the chalcogens (X = S, Se, Te) in the form of MX_2 as shown in Figure 2. TMDCs are 2D nanomaterials consist of a monolayer of transition metal atoms sandwiched (X-M-X) between two layers of chalcogen atoms (usually selenium, sulfur, or telluride) in a hexagonal lattice[6].

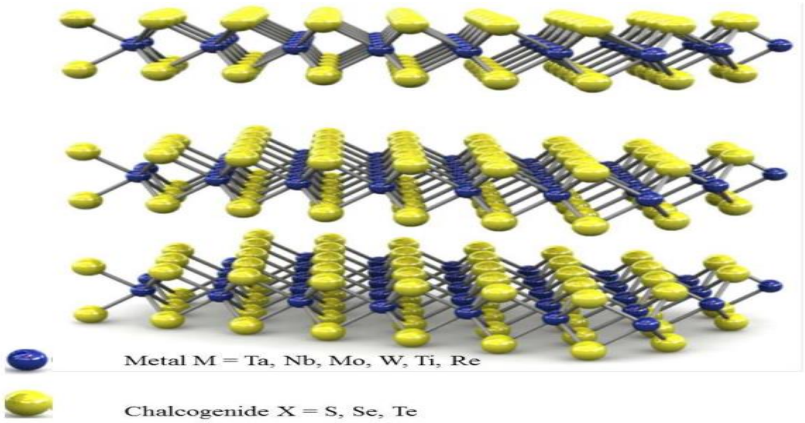

Figure 2. 2D Transition metal dichalcogenides[6]

TDMCs can take in various crystal structures. The most common is the 2H-phase with trigonal symmetry, which results in semiconducting features such as MoS_2, WS_2, $MoSe_2$. These semiconductors, when in bulk, have an indirect bandgap. The bandgap becomes direct for monolayers and in the visible spectrum, making them attractive to optoelectronics.

TMDCs, including MoS2 and WS2, are attractive in this regard due to their ultra-thin structure and inimitable electronic band structures with unique features, including indirect-to-direct band-gap transition[10] and nondegenerate doping[11]. Furthermore, both MoS_2 and WS_2 have a light absorption coefficient that is about one order of magnitude higher than that of conventional 3-d semiconductor Si[12]. The performance of a solar cell depends on optimal bandgap and a high absorption coefficient of the absorber material. Thus, to realize the highly efficient optoelectronic devices based on 2D TMDCs semiconductors, it is important to develop a strategy to tailor their bandgap as well as absorption coefficient over the entire solar spectra. But WS_2 bulk TMDCs show indirect bandgap semiconducting behavior while 2D monolayer of these materials show direct bandgap semiconducting behavior[13].

In the direct bandgap semiconductors, minimum energy of the conduction band lies directly above the maximum energy of the valence band in momentum space. Electrons at the conduction-band minimum can combine directly with holes at the valence band maximum, while conserving momentum. In the indirect bandgap semiconductors, the momentum of the conduction band minimum and valence band maximum is not the same, so a direct transition across the bandgap does not conserve momentum and is forbidden. Recombination occurs with the mediation of a

third body, such as a phonon or a crystallographic defect[14], which allows for conservation of momentum. The energy difference between the photon energy and the bandgap energy of the photovoltaic material is a main factor of energy loss. When photon energy is smaller than the bandgap energy, there will be no absorption. If the photon energy is much greater than the bandgap energy and equal to the bandgap energy will be absorbed and the other part will be wasted as heat.

1.2 Why 2D Materials?

The following three points describe why 2D materials are important.

Removal of vdW interactions: A layered bulk material is made up of many covalently bonded planes which are held together by weak vdW interactions. This vdW forces can be easily overcome when a force is applied to a material and the material breaks-making it weak. Conversely, the covalent bonds in the layers which hold the atoms together are actually very strong. Covalent bonds are present in monolayers and monolayers appear stronger by removing the 'weak links' from the bulk material.

An increase in the Surface-to-Volume ratio: A material's Surface-to-Volume ratio defines how much of it is exposed to its environment. This is important for chemical reactions, the more reactant that is in contact with the material, the faster the reaction can occur, thus 2D materials tend to be more reactive than their bulk counterparts.

Confinement of electrons in a plane: The electronic and optical properties of a material depend on its structure of the electronic band structure. This describes how electrons move through the material, and is the result of its crystal structure periodicity. When a material goes from bulk to 2D, the periodicity is removed in a perpendicular direction to the plane, which can change the band structure.

1.3 Application of 2D Materials

2D TMDCs have special electrical and optical properties arising from quantum confinement and surface effects resulting from the transition from indirect bandgap to direct bandgap as bulk materials are scaled down to monolayers. This tunable bandgap in TMDCs making them promising candidate for a variety of opto-electronic devices, including solar cells, photo-detectors, light-emitting diodes, and photo-transistors[8].

Sheet-like structures, vdW gaps between each adjacent layer, and large specific surface area are distinct features that make 2D TMDCs highly desirable for capacitive energy storage (e.g. supercapacitors and batteries) and sensing applications[15].

The atomic layers of the weakly bonded 2D TMDCs is that they can be conveniently isolated and stacked with other TMDCs to create a wide range of vdW heterostructures without the constraint of matching lattices. For example, stacking together one-atom-thick sheets of dissimilar TMDCs, vertically stacked heterostructures enables unique functions and superior properties to be realized that cannot be obtained otherwise[16],[17],[18]. Figure 3 shows different devices constructed from the 2D TMDCs and their application areas.

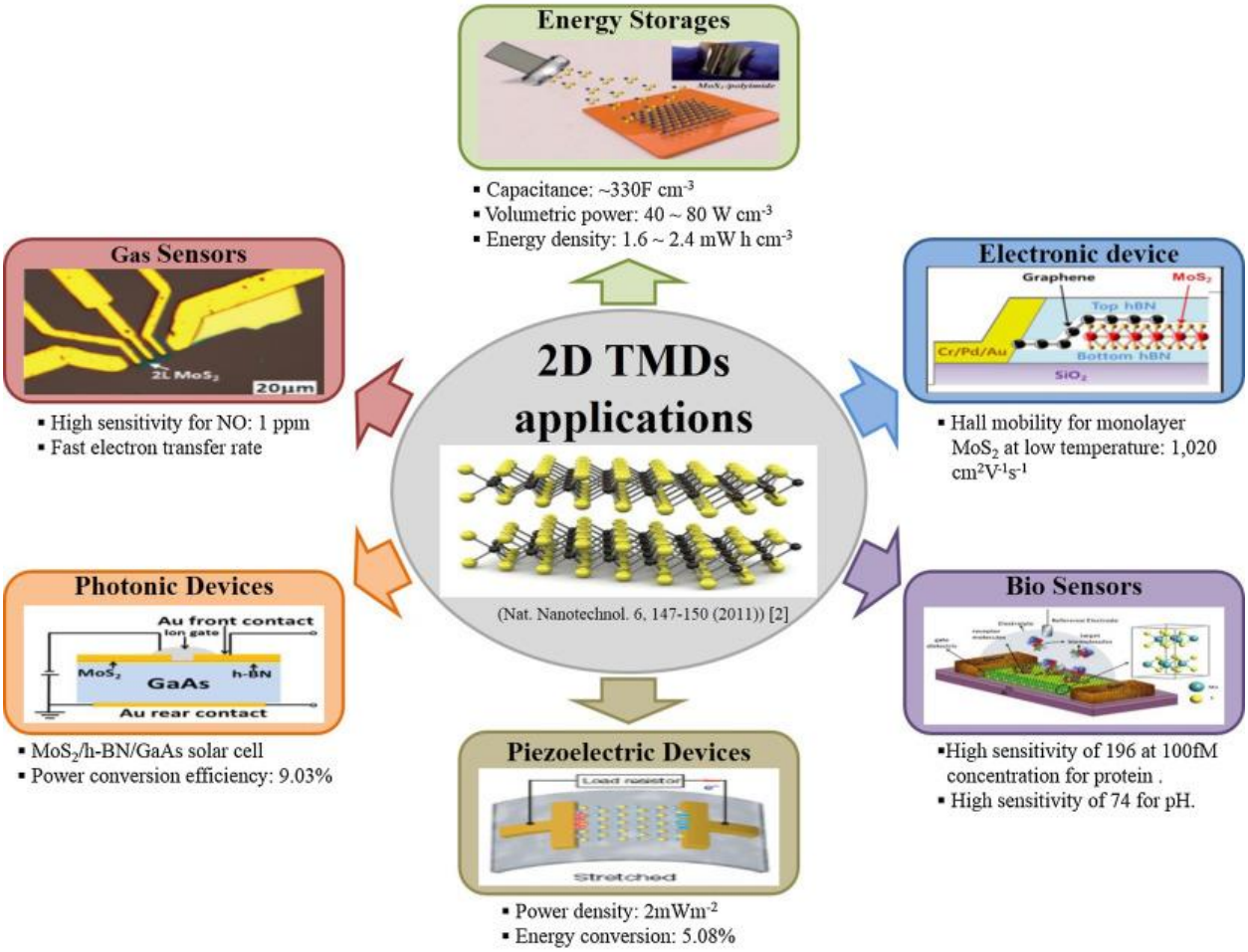

Figure 3.Devices constructed from the 2D TMDCs by using their unique physical, chemical, and optoelectronic properties [8]

1.4 Objectives

1.4.1 General objective

The general objective of this work is to investigate the electronic structure and properties of WS_2 and JTMDs monolayer heterostructures for PV devices using Density Functional Theory.

1.4.2 Specific Objectives

The specific objective of this research is:

- To determine the band structure and DOS of monolayer WS_2 and JTMDs
- To build WS_2/JTMDs heterostructures, optimize and check different stacking patterns
- To determine band structure, DOS band alignment and electrostatic potential difference of the heterostructures

1.5 Scope of the Study and Limitation

The study covers investigation of electronics structure and properties of JTMDs/WS_2 heterostructures based on DFT. The scope of this study is only on the theoretical properties based on DFT without any experimental work.

GGA-PBE approximation was only used in this study and this approach underestimates the electronic properties of the heterostructures. Other approaches that give better electronic properties such as HSE06 were not employed due to lack of supercomputer and time limitation.

2 Literature Review

Recently, 2D TMDCs, such as MoS_2, WS_2 and others, have been widely studied for their excellent properties in mechanics, electronics, optics and many more[19]. WS_2 has gained considerable attention as a typical 2D TMDCs material for its extensive prospects of application in electronics[19]. In our calculations WS_2 monolayer is a direct gap with a bandgap of approximately 1.8 eV. Simple monolayer WS_2 has a distinctive layered structure and consists of a sandwich structure S – W – S. The single-layer TMDCs possess high carrier mobility, good flexibility and transparency, makes them ideally suited for the fabrication of high-performance nanoelectronics and optoelectronic devices[20]. Due to its significant chemical and physical properties, has attracted considerable interest. It has a 1.3–2.2 eV bandgap, within the range of PV materials, which makes it attractive for such applications[21] .

2.1 Structure and properties of Monolayer WS_2

Tungsten Disulfide (WS_2), a TMDC is an important 2D layered material which has attracted a great deal of interest because of its significant chemical and physical properties. WS_2 has a trigonal prismatic structure in which each layer is composed of a layer of hexagonally arranged W atoms sandwiched between two layers of hexagonally arranged S atoms[21]**.** Its 2D layered structure makes it possible to modify and tune its electronic properties by doping with other atoms or molecules between weakly bonded layers. There are strong W-S covalent bonds within a layer, while adjacent layers are held together by weak van der Waals**'** forces[22]. Depending on the arrangement of the atoms, the structures of 2D TMDCs can be categorized as trigonal prismatic (hexagonal) structure. Typical atomic ratio in layered TMDCs exhibits one transition metal to two chalcogen sulfur atoms to create WS_2. Therefore, chalcogen–metal–chalcogen arrangement along Z-direction is considered as single layer, and weak vdW interactions between each layer (chalcogen–chalcogen) enable mechanical exfoliation from bulk TMDCs to obtain single layer.

WS_2 has a bandgap of 1.3**–**2.2 eV, well within the range of photovoltaic materials, which makes it attractive for these applications. A primitive unit cell consists of one W atom and two S atoms in a trigonal prismatic configuration. Like other TMDCs, WS_2 has significant absorption of incident photons with energies above its bandgap, make it a good absorber.

2.2 Structure and Properties of JTMDs Monolayer

Atomically thin Janus transition metal dichalcogenide (JTMDs) with an asymmetric structure have emerged as a new class of intriguing 2D semiconductor materials. Janus MoSSe, MoSTe, MoSeTe, WSSe, WSeTe and WSTe as new members to the family of transitional metal dichalcogenides (TMDCs) present intriguing properties that absent in its parent MX_2 (M = Mo, W; X = S, Se, Te) monolayers due to the out-of-plane mirror asymmetry. Using state of the art density functional theory (DFT) calculations electronic properties of JTMD monolayers with a band-gap range from 1.37 to 1.96 eV[20].

2.3 An Overview of 2D vdW Heterostructure

After the discovery of graphene in 2004, the scientific community has discovered more than 2500 other layered atomically thin 2D materials. Although these materials cover an enormous range of electrical, chemical, optical and mechanical properties, perhaps the most surprising discovery is that these crystals can be freely combined to produce entirely new materials. They find that when two atomically thin graphene-like materials are placed on top of each other their properties change, and a material with novel hybrid properties emerges that paves the way for the development of new materials and nano-devices. The properties of this hybrid material can be precisely controlled by twisting the two stacked atomic layers, thus opening the way for the use of this unique degree of freedom in future technologies for the nanoscale control of composite materials and nano-devices. While strong covalent bonds provide in-plane stability of 2D crystals, these materials are called van der Waals heterostructures because the atomically thin layers are not mixed by a chemical reaction but rather attached to each other via a weak so-called van der Waals interaction.

To build vdW heterostructures for the realization of advanced electronic, optoelectronic and photovoltaic devices a wide range of 2D materials ranging from semi metals to insulators have been used. Consequently, considering different stacking or combination patterns, the range of application of 2D TMDCs could be broadly extended. In particular, 2D TMDCs can be vertically stacked layer by layer, forming the van der Waals (vdW) heterostructures[23].

The large combinatorial library of 2D materials constitute it a feasible way to design advanced heterojunctions without the concern of lattice mismatch by restacking various 2D layers[18] as show in Figure 4.

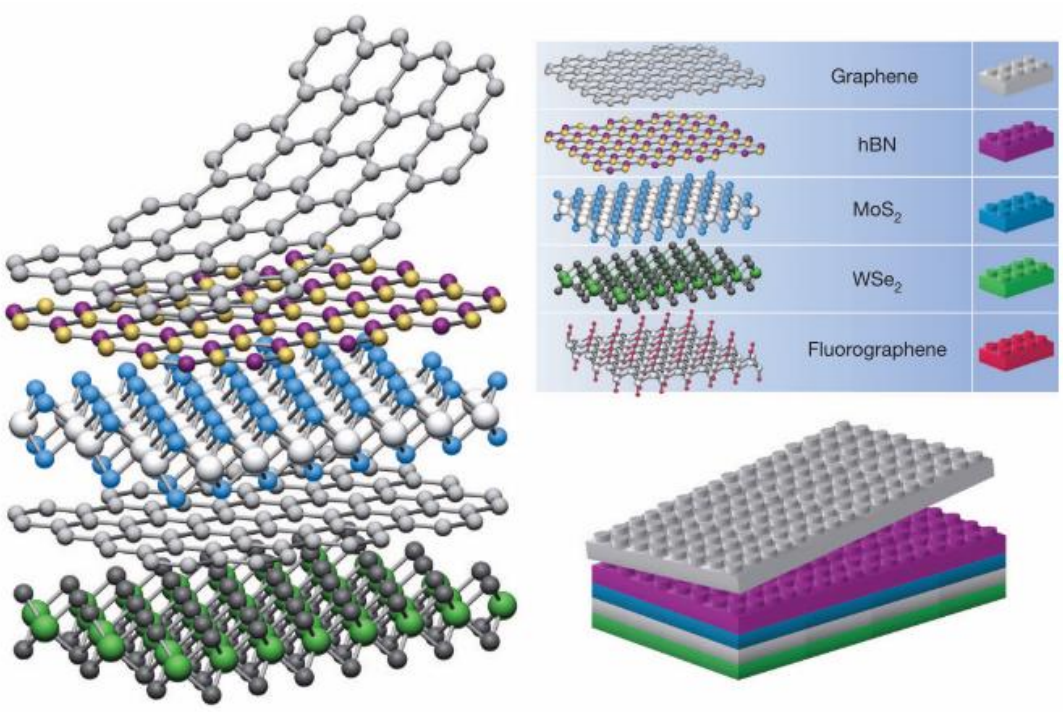

Figure 4. Building van der Waals heterostructures [18].

Three forms of heterojunctions (type I, II, and III) can be easily constructed with selectable materials based on the various combinations of band alignments depending on the energy difference of the conduction and valence-band extrema in the constituent layers as show in the Figure 5.

The valence band maximum (VBM) and the conduction band minimum (CBM) of two independent components are located on the same side of the heterointerface for Type I (straddling gap) heterojunctions, and the radiative recombination is enhanced because both electrons and holes reside in one material. Type-I heterojunctions have the structure of a quantum well, making them promising applications for optoelectronic devices such as light-emitting diodes (LEDs) and in type-II (staggered gap) heterojunctions, the CBM and VBM belong to two separate components with different work functions, providing opportunities to modulate the interlayer transition energy and induce the charge spatial separation. Hence vdW type II heterostructures carry great promise for high-performance optoelectronic applications. Most of the 2D TDMCs in general usually form

type II junctions. In heterojunctions of type III (broken gap), the VBM of one semiconductor is greater than that of the other semiconductor.

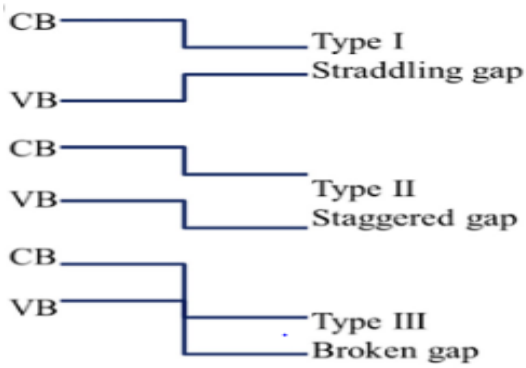

Figure 5. Schematic energy band diagrams of the three types of semiconductor heterojunctions: type-I(straddling gap),type-II(staggered gap),and type-III(broken gap)heterojunctions[18].

Weak vdW interaction between two types of stacked 2D materials, potentially play a critical role in influencing the electronic properties of the neighboring 2D layers. 2D vdW heterojunctions with high quality heterointerfaces enables the efficient charge separation after photo-excitation, holding great potential for ultrathin and ultralight photovoltaic applications[24].Theoretically estimated that the power conversion efficiency (PCE) based on 2D materials could exceed 25%[25], which is competitive with conventional solar cells.

2.3.1 Photo Voltaic Based on 2D vdW Heterostructures

2D vdW heterojunctions with high-quality hetero interfaces allow efficient charge separation after photo-excitation, providing great potential for PV ultrathin and ultralight applications. From material science point of view of, 2D materials can be designed for: (i) strong light absorption in the UV as well as in the solar spectrum VIS region; (ii) suitable electronic level alignment for high open circuit voltage and heterostructure donor/acceptor interface; (iii)high charge carrier (electrons and holes or excitons) mobility to guarantee effective charge separation and collection[26]. Recombination of charge should be avoided as far as possible and thus the electronic band structure and band alignment at interfaces also play a key role in this aspect.

Combining different work functions of materials can lead to photo excited electrons and holes accumulated in different layers, giving rise to indirect excitons[27]. These excitons usually have long lifetimes, and their binding energy could be controlled by tuning the distance between the semiconductor layers. Table 1 shows PVs from different 2D vdW heterostructures. Four vdW

heterostructures have good ability to absorb the visible and near infrared (NIR) light, which is indicated by the absorption peaks of MoS_2/BP, $MoSe_2$/BP, WS_2/BP and WSe_2/BP vdW heterostructure. These 2D vdW heterostructures are promising for various photocatalytic, PV, and optical devices because the wavelength of light at earth is mostly in the NIR and visible regions[28].

S. Roy and et al. studied the electronic and optical properties of bulk WS_2/WSe_2 and Janus WSSe/WSeTe structure using hybrid computational approach based on DFT and obtained maximum efficiency values of 17.73% and 18.87% for AZO/WSSe/WS_2 and AZO/WSSe/WSe_2 solar cells, respectively[29]. Again, S. Roy and et al. reported a maximum efficiency using a combination of monolayer WS_2, bulk WS_2 and amorphous silicon (a-Si) using numerical calculations and simulations[21] as shown in the Table-1. The performance of this solar cell is comparable to many commercial cells. The results show how monolayer WS_2 can serve as a suitable PV material. GaSe/GaTe heterostructure is also another potential candidate for the application of high efficient solar cell[30], opening possibilities to develop solar cells based on 2D TMDCs.

Table 1: Important terms for a photovoltaic device

Terms	Definition
Power conversion efficiency (PCE)	The ratio of electrical power generated by the device to the incident light power on it.
Short-circuit current ($\mathbf{I}_{sc}$)	Current flowing through the device under illumination and at zero external bias with its contacts shorted.
External quantum efficiency (EQE)	The ratio of the number of charge carriers flowing through the device under short-circuit current conditions to the total number of impinging photons on it.
Open-circuit voltage ($\mathbf{V}_{oc}$)	The voltage generated by the device under illumination and with no current flowing.
Fill factor (ff)	The ratio of the maximum electric power generated by The device to the product of it short-circuit current and its open-circuit voltage.

Table 2: Summary of 2D vdW heterostructure based photovoltaics

Device configuration	EQE	optical absorbance	Voc(V)	Bandgab(eV)	η%	Reference
WSe_2/WS_2	50.2%		0.58	1.8	2.4%	[26]
LWS_2/BWS_2/a-Si	85%		0.843 V		23.26 %	[21]
WS_2/p-Si	60%		16.34 mV			[31]
GaSe/GeS		10^5 cm^{-1}		1.8	16.8%	[30]
GaSe/GaTe				1.2	18%	
AZO/WSSe/WS_2	85%		0.8		17.73 %	[32]
AZO/WSSe/WSe_2	85%		0.6		18.87 %	
MoS_2/BP		16.59×10^5 cm^{-1}		1.29		
$MoSe_2$/BP				1.37		
WS_2/BP		$16.82\times10^5 cm^{-1}$		1.22		[28]
WSe_2/BP		18.21×105 cm^{-1}		1.21		
		$18.71\times10^5 cm^{-1}$				
MoS_2/GaN		5.5×10^5 cm^{-1}		1.79 eV		
MoS_2/AsP	71%				9%	[33]
MoSSe/WSSe				1.08		[23]

EQE: external quantum efficiency; η**:** power conversion efficiency (PCE); L: layered; B: bulk

Currently available Solar cells are not cost effective, and their efficiency is restricted by the Shockley–Queisser limit. There are many progresses made in the previous studies. However, there are still problems in the production cost, manufacturing time, life time of minority carriers, efficiency and thickness of solar cells. In addition, energy losses (transmission loss and thermalization) highly affect the efficiency of solar cells.

Because of their unique optical, electronic, high-quality and mechanical properties, 2D nanomaterials are promising candidates for developing cost-effective, simple manufacturing processes, ultra-thin, low-temperature coefficient and efficient PV devices through integration with conventional bulk semiconductors.

In this study, the band structure and DOS of WS_2 and JTMDs monolayers were calculated and JTMDs and WS_2 monolayer materials were combined to obtain layered 2D JTMDs/WS_2 heterostructures. The electronic properties of JTMDs/WS_2 monolayer heterostructures are studied using first-principles calculations based on DFT. DFT calculations show a significant difference in bandgap between the heterostructure and each monolayer WS_2 and JTMDs. It is predicted that the JTMDs monolayers can be a potential channel to slightly change the electronic properties of pristine WS_2, which can be used in the design of PVs**.** In this study, band structure, DOS, and band alignment of new types of JTMD/WS_2 heterostructures were addressed.

3 Methodology

3.1 Basics of Theory and Approximations used

This chapter contains a detailed description about the implementation of First Principle Calculation in order to understand the electronic structure of new materials. The advanced and accurate knowledge of materials especially at atomic and molecular levels are essential for performing various desired technological functions bringing about revolution in modern day life. Where classical mechanics fails, quantum mechanics provides the correct description of materials. For a bulk system one needs to take into account a large number of degrees of freedom to describe a huge number of electrons and atomic cores and has to solve the many-body Schrödinger equation for interacting electrons and nuclei in order to grasp knowledge about the electronic behavior of materials. But most of the many-body quantum mechanical problems are either impossible or very difficult to solve.

Progress in computational materials science with the development of variety of computational methodologies has opened up a number of new horizons regarding exploration of material properties having at most technological importance. A wide range of material properties can be predicted with great precision before executing the experimental investigation, which could avoid expensive, tedious and time-consuming exercise. While predicting a certain property, designing a novel material or investigating its characteristic properties at atomic level computational material science has been proved to be significant importance. The trend in designing functional materials with reduced(nanometer) size consisting of few hundreds of atoms only and to improve the accuracy, it has become inevitable to go beyond the previously used. To make this difficult task tractable, the DFT comes in to picture to investigate the properties of novel functional nanostructures.

For the last few years DFT has been the dominant and most successful method for the quantum mechanical simulation of periodic systems. DFT is the key step towards the development of independent-particle methods for solving many-body problems. It includes tools like the local density approximation (LDA) and followed by an approximation providing improved structural and magnetic properties, the GGA which turned out to be very successful for studying the electronic structures of materials.

The theoretical foundation for this promising approach was originated by P. Hohemberg and W. Kohn in 1964 by assigning density as a 'basic variable' and deriving all other features of the material as functional of its ground state electron density. In this thesis, the detailed analysis of band structure calculation and density of state DOS calculation has been discussed for monolayers WS_2, MoSSe, WSSe, MoSTe, MoSTe, MoSeTe, WSeTe and heterostructures of JTMDs/WS_2. Finally, in order to study the photovoltaic applications, the electronic properties and the band alignment has been analyzed for JTMDs/WS_2 monolayer heterostructures. The calculations have been done using Quantum ESPRESSO and VASP. These software's use self-consistent calculation to solve the Schrödinger equation for many body systems.

3.1.1 Many body problems

The many-body problem is a general name for a physical problem pertaining to the properties of quantum systems made of many interacting particles including condensed physics.

In order to study the electronic structure properties in solid state physics, which generally have large number of atoms (**$\sim 10^{23}$**) the solution of many body problems become inevitable. The problem is determining the state of the electrons in a system with fixed atomic nuclei. Since direct numerical solution of the many-body Schrödinger equation is intractable even for systems of moderate size. While studying such systems, where large number of atoms (many electrons and nuclei) interacts with each other, their properties can be determined by solving the Schrödinger equation.

$$H\psi(r, R) = E\psi(r, R) \qquad (3.1)$$

The Hamiltonian is

$$H = -\sum_i \frac{\hbar^2 \nabla_i^2}{2m_e} - \sum_I \frac{\hbar^2 \nabla_i^2}{2M_I} + \frac{1}{2}\sum_{i \neq j} \frac{e^2}{r_i - r_j} + \frac{1}{2}\sum_{i \neq j} \frac{Z_I Z_J e^2}{R_i - R_j} - \sum_{i,I} \frac{Z_I e^2}{r_i - R_I} \quad (3.2)$$

Where in equation 3.1 the term $\hbar = \frac{h}{2\pi}$represents reduced Planck's constant m_e, r_i and e are the mass, position, and charge of the electron i^{ith} respectively. Where M_I, R_I and $\boldsymbol{Z_I}$ represents the mass, position, and charge of the I^{ith} nuclei respectively. The first two terms give the kinetic energies of electron and nuclei whereas the remaining terms represents the electron-electron, nuclei-nuclei and electron-nuclei interactions respectively.

For any other system consisting of large number of electrons and nuclei, it is inevitable to employ some approximations, even for helium. One of the most extensively used approximation method in almost all the methodologies is Born Oppenheimer approximation[34].

Let us consider the wave functions of both the electron and nuclei separately. As the motion of electron is much greater than that of nuclei due to its larger mass, so we can consider the nuclei as stationary. Then the kinetic energy of nuclei can be neglected due to its frozen equilibrium state.in this case the nuclei considered as external potential V_{ext} applied to moving electrons and then the wave functions of electrons ψ_e (r, R) and the nuclei $\psi_N(r, R)$ becomes

$$H\psi(r, R) = \psi_e(r, R)\,\psi_N(r, R) \qquad (3.3)$$

And the Schrödinger equation for only electrons will take the form

$$H_e\psi_e(r, R) = E_e\psi_e(r, R) \quad (3.4)$$

After applications of Born Oppenheimer application, the Hamiltonian will be

$$H = -\sum_i \frac{\hbar^2\nabla_i^2}{2m_e} + \frac{1}{2}\sum_{i\neq j}\frac{e^2}{r_i - r_j} - \sum_{i,I}\frac{Z_I e^2}{r_i - R_I} \quad (3.5)$$

The electron-electron interaction represented by the three term as shown in the equation 3.5 needs further application, it cannot be solved with this application only. In order to deal with this problem other approximation like Density functional theory (DFT) has been applied.

3.1.2 Hohenberg-Kohn Theorems

The theorems of Hohenberg-Kohn played an important in density functional theory of many-body systems. An interacting system in an external potential can be visualized using DFT with the help of the two famous theorems provided by Hohenberg and Kohn in 1964. The external potential (and hence the total energy), is a unique functional of the electron density.

Hohenberg-Kohn Theorem I:

The external potential is a unique functional of the electron density in the ground state, and therefore the total energy is also a functional of the ground state electron density. A consequence of the first Hohenberg-Kohn theorem is that all properties of a system are determined from only the ground state electron density.

Proof:

We proceed by using reference[35].We have a ground state electronic wave function ψ that gives an electron density n(r) for an external potential v(r).Assume we have a second external v'(r)potential that has a ground state ψ' which gives the same density n(r). The corresponding Hamiltonian and ground state energy for ψ, ψ 'are H, H' and E, E', respectively. As ψ 'is not the ground state of H, we can say that:

$$E = \langle\psi|\hat{H}'|\psi\rangle < \langle\psi'|\hat{H}'|\psi'\rangle = \langle\psi'|\hat{H}'|\psi'\rangle + \langle\psi'|\hat{H} - \hat{H}'|\psi'\rangle \quad (3.6)$$

$$= E' + \int [v(r) - v'(r)]n(r)dr \quad (3.7) \text{ so we have:}$$

$$E < E' + \int [v(r) - v'(r)]n(r)dr \quad (3.8)$$

If the unprimed and primed indices are reversed, we also have:

$$E' < E + \int [v'(r) - v(r)]n(r)dr \quad (3.9)$$

Addition of equations 3.8 and 3.9 leads to the contradiction:

$$E + E' < E' + E \quad (3.10)$$

So, to within a constant, the external potential v(r) is a unique functional of the ground state electron density n(r)as was set out to be shown.

Hohenberg-Kohn Theorem II:

The total energy of a system, which is a functional of the ground state electron density through the first theorem, is minimized for the correct ground state energy. Hohenberg and Kohn defined a universal functional that is valid for any system of electrons, regardless of the external potential. For a given external potential, v(r), we have the total energy functional E[n] as:

$$E[n] = F[n] + \int v(r)n(r)dr \quad (3.11)$$

Where we neglect the energy from the interaction of the nuclei. The universal functional F[n] includes all of the electronic energy:

$$F[n] = T[n] + V_{ee}[n] \quad (3.12)$$

Where we have the kinetic energy functional T[n] and the potential energy functional $V_{ee}[n]$ from electron-electron interactions.

For a system with a ground state electron density n(r), the ground state energy E is equivalent to the total energy functional E[n], which is equal to the expectation value of the Hamiltonian for the ground state wave function ψ, thus:

$$E = E[n] = \langle \psi | \hat{\mathrm{H}} | \psi \rangle \qquad (3.13)$$

For a different density n'(r) with wavefunction ψ' it follows from the variational principle that the energy corresponding to this state, E' is greater than the ground state energy:

$$E = \langle \psi | \hat{\mathrm{H}} | \psi \rangle < \langle \psi' | \hat{\mathrm{H}} | \psi' \rangle = E' \qquad (3.14)$$

Therefore, the total energy functional E[n] gives the exact ground state energy only for the exact ground state density. If the universal functional F[n] is known, then the total energy can be minimized with respect to n(r) and the exact ground state electron density and total energy would be found. Simple yet powerful as the Hohenberg-Kohn theorems are, they do not provide a route to construct functional or a method to calculate the ground state density.

3.1.3 Kohn Sham equation

In 1965, Kohn and Sham showed that it is possible to reduce the many body quantum mechanical problem to an exactly equivalent set of one electron equations, solved self consistently. This is a reformulation of the following idea. The system of interacting electrons is mapped on to an auxiliary system of non-interacting electrons having the same ground state charge density n(r). In Kohn Sham equation the Schrödinger's equation for the system takes the following form:

$$\left[\frac{\hbar^2 \nabla_i^2}{2m} + V(r)_{ion} + V(r)_H + V_{XC}[n(r)]\right] \varphi_i(r) = \varepsilon_i \varphi_i(r) \quad (3.15)$$

The first term is the energy of non-interacting electrons. The second term $\mathbf{V(r)}_{\text{ion}}$ is the ionic potential describing the attractive interaction between electrons and nuclei. The third term (called the Hartree potential) contains the electrostatic interactions between clouds of charge**.**

$$V(r)_H = \int \frac{n(r)' e^2 d^3 r}{|r_i - r_j|} \qquad (3.16)$$

The fourth term is called the exchange and correlation potential.

$$V_{XC}[n(r)] = \frac{\delta E_{xc}}{\delta n(r)} \qquad (3.17)$$

Ground state electronic energies $\varepsilon_i$and wave functions$\varphi_i = |i, k$can be obtained as the result of the DFT calculation.

If each term in the Kohn-Sham energy functional was known, we would be able to obtain the exact ground state density and total energy. Unfortunately, there is one unknown term, the exchange-correlation (xc)functional (E_{xc}). E_{xc} includes the non-classical aspects of the electron-electron interaction along with the component of the kinetic energy of the real system different from the fictitious non-interacting system. Since E_{xc} is not known exactly, it is necessary to approximate it, which is the focus of the next section. In many cases very good agreement with experiment is achieved when the exchange and correlation potentials applied Approximations like LDA or GGAs are widely used to study IV and II-V semiconductors and also insulators and cases where electrons have stronger effects of correlations (transition metals).

3.1.4 Exchange Correlation Functional

The only unknown term is the exchange correlation functional term, which needs to be approximated in order to use Khon sham equation for practical purposes.

For practical purpose use of the Kohn-Sham equations we must know what form of the exchange-correlation energy functional is. However, the exact form of E_{xc} is not known and may never be known (in a closed mathematical form). Thus, since the birth of DFT some sort of approximations for E_{xc} have been used. By now there is an almost end-less list of approximated functional with varying levels of complexity.

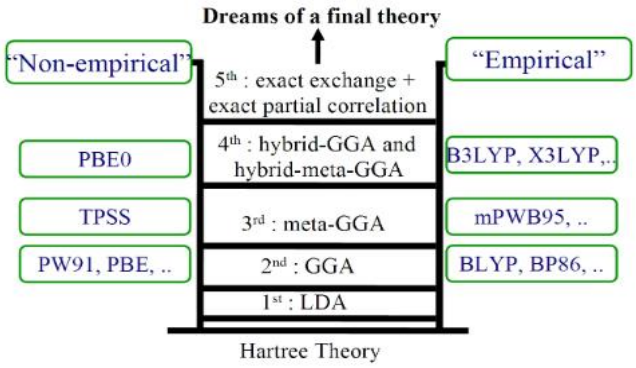

Figure 6. Schematic diagram of "Jacob's ladder "of exchange-correlation functionals proposed by J. P. Perdew.

Useful way to present the many and varied Exc functional that exist has been proposed by Perdew and is known as "Jacob's ladder" (Figure 6)[36]. In the diagram above the E_{xc} are grouped according to their complexity on rungs of a ladder which lead from the Hartree approximation on

"earth" to the exact exchange-correlation functional in "heaven". The E_{xc} also categorized in to non-empirical (formulated only by satisfying some physical rules) and empirical (made by fitting to the known results of atomic or molecular properties). The first few rungs of this ladder are now briefly discussed approximations like LDA or GGAs are widely used to study IV and II-V semiconductors and also insulators and cases where electrons have stronger effects of correlations (transition metals).

3.1.4.1 The local-density approximation (LDA)

In this approach a real inhomogeneous system is divided into infinitesimal volumes, and the electron density in each of the volumes is taken to be constant. The exchange-correlation energy for the density within each volume is then assumed to be the exchange-correlation energy obtained from the uniform electron gas for that density. Thus, the total exchange-correlation energy of the system can be written as

$$E_{xc}^{LDA}[n] = \int n(r)\varepsilon_{xc}^{unif} n(r)dr \qquad (3.18)$$

Where ε_{xc}^{unif} is the exchange-correlation energy per particle of the interacting uniform electron gas of density n(r).

LDA is powerful in describing many properties of systems. In inhomogeneous systems LDA underestimates correlation but overestimates exchange, resulting in unexpectedly good values ofE_{xc}^{LDA} and also the assumption that the electron density around an atom to be homogeneous.

3.1.4.2 Generalized Gradient Approximation (GGA)

It was realized very early that only the local uniform density at each given point is not a reasonable approximation for the rapidly varying electron densities of many materials, and that the gradient of the density (∇n(r)) needs to be included. The exchange correlation can be written in terms of many functions:

$$E_{xc}^{GGA}[n] = \int \varepsilon_{xc}^{GGA}(n(r)|\nabla n(r)|)n(r)dr \qquad (3.19)$$

This is called "Generalized Gradient Approximation" which often deals with structural and magnetic properties of materials with great accuracy. Many functions have been implemented so far and worked successfully. There are two commonly used functionals in calculations involving solids. These are the Perdew Wang functional (PW91) and the Perdew Burke Ernzerhof

functional (PBE) (The Perdew–Burke–Ernzerhof functional (GGA-PBE) is employed to treat the exchange and correlation potentials in this thesis.

3.2 The plane wave pseudopotential method

The plane wave pseudopotential (PWPP) method is one of the most widely used implementations the Kohn-Sham formulation of DFT.

3.2.1 Plane Waves as a Basis

When studying the electronic structure of condensed matter systems, one is investigating the behaviour of a number of electrons in the order of 10^{28} per mole of atoms. Many extended systems are periodic in structure, corresponding to one of the Bravais lattices, so one can define an infinite periodic system and perform calculations for only the electrons in the periodic cell. Bloch's theorem shows that the wavefunction ψ, of an electron in bands, for a periodic system can be expressed as a combination of a plane wave part and a periodic cell part[37]:

$$\psi_n(r) = u_n(r)e^{ikr} \qquad (3.20)$$

Where the plane wave part has wave vector k, which is confined to the first Brillouin zone. The periodic part has the same periodicity as the lattice.

$u_n(r + R) = u_n(r)$, where R is one of the lattice vectors.

This leads us to choose a plane wave basis set to describe the wavefunction within the periodic cell. The periodic part of the wavefunction can then be written as:

$$u_n(r) = \sum_G C_n, G e^{iGr} \qquad (3.21)$$

Where we have plane wave coefficients c_n and G are the reciprocal lattice vectors that satisfy the relation $G = 2\pi m$ where m is an integer. If we combine equations 3.20 and 3.21, the Kohn-Sham orbitals can therefore be written as an infinite sum of plane waves:

$$\psi_n(r) = \sum_G C_n, (K + G)e^{i(K+G).r} \qquad (3.22)$$

Where Cn, k+G the coefficients of the plane waves describing the wavefunction.

Bloch's theorem allows us to take an infinite system but only calculate a finite number of electronic wavefunctions. However, this leaves an infinite number of k-points as each electron occupies a

definite K. In practice, we need only choose a sample of k-points as the wavefunction varies slowly over small regions of k-space. The electronic wavefunctions at k-points that are close will be nearly identical. Therefore, a region of k-space can be represented by the wavefunction at a single k-point. K-point sampling schemes have been developed, such as the one given by Monkhorst and Pack[38]. The symmetry of the lattice can be used to reduce the number of k-points required. The Brillouin zone can be made irreducible by applying the point group symmetries of the lattice, leaving no k-points related by symmetry.

The sum over G vectors in equation is infinite in order to fully describe the wavefunction, i.e. for the plane wave basis set to be complete. When devising a computational implementation, one must choose a finite end to the sum. For most realistic wavefunctions, there will be a scale below which the wavefunction can be described as smoothly varying. This means that the coefficients

Cn, k+G will become small for large K+G.

The cutoff point is referred to as the plane wave kinetic energy cutoff:

$$E_{cut} \geq \frac{1}{2}|K+G|^2 \qquad (3.23)$$

I.e. it is greater than or equal to the highest kinetic energy of the plane waves used. This corresponds to a sphere in reciprocal space within which all the used K+G vectors lie. When performing calculations, one must always be careful to select an appropriate sampling of k-points and plane wave cutoff energy. This is done by performing calculations at successively higher cutoff energies and finer grids of k-points until the quantities of interest no longer change on the test of convergence.

3.2.2 The Pseudopotential Approximation

Electrons in the vicinity of the nuclei will be under the influence of a steep Coulomb potential and have rapidly varying wave functions in the nuclear regions. This requires a correspondingly large number of plane waves to adequately describe the wave function and the nuclear potential.
In general, there are two main purposes of the pseudopotential formalism. First, to use a much weaker pseudopotential to get rid of core electrons which due to their deep potential would need to be described by many plane-wave basis functions. Second, to eliminate the rapid oscillations of the valence electron wavefunctions in the core region.

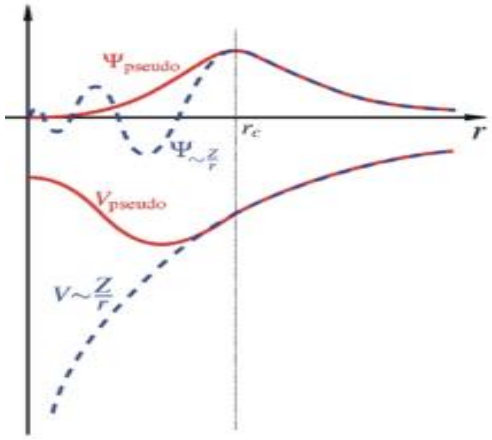

Figure 7. Schematic illustration of all-electron (dashed lines) and pseudopotential (solid lines) and their corresponding wave functions. The radius at which the all-electron and pseudo-electron values match is designated as r_c.

Different computational tools were used to answer the research question in this study such as, Quantum-ESPRESSO, VASP, Materials Studio and VESTA.

3.3 The Quantum-ESPRESSO Software

Quantum-ESPRESSO is a distribution of software for atomistic based on electronic structure, using density-functional theory (DFT), a plane waves (PW) basis set and pseudopotentials (PP). Quantum-ESPRESSO is distributed for free software under the GNU General Public License and stands for Quantum opEn-Source Package for Research in Electronic Structure, Simulation, and Optimization[39], [40].

3.4 VASP

VASP is a complex package for performing ab-initio quantum-mechanical molecular dynamics (MD) simulations using pseudopotentials or the projector-augmented wave method and a plane wave basis set. The approach implemented in VASP is based on the (finite temperature) LDA with the free energy as variational quantity and an exact evaluation of the instantaneous electronic ground state a teach MD time step[41]. Electronics properties of the heterostructures are calculated by using VASP.

3.5 Materials Studio and VESTA

To build bilayer heterostructure JTMDs and WS_2 used Materials Studio and VESTA. Materials Studio is a complete modeling and simulation environment designed to allow researchers in materials science and chemistry to predict and understand the relationships of a material's atomic and molecular structure with its properties and behavior[42] and VESTA is a 3D visualization system for structural models, volumetric data and crystal morphologies[43].

3.6 The Plane-wave self-consistent field method

In second chapter, we have seen the set of Kohn-Sham equations is strongly non-linear and it is an iterative method in order to solve it. The interaction between a given particle and the other particles of a quantum-mechanical system consisting of many particles. Around the two main programs PWscf, Quantum ESPRESSO is developed, used to preform self-consistent calculations. Many interacting particles have a very complex problem and have no exact solution, calculations are performed using approximate methods. One of the most often used approximate methods of quantum mechanics is based on the introduction of a self-consistent field, which permits the many-particle problem to be reduced to the problem of a single particle moving in the average self-consistent field produced by the other particles. The different schemes for the introduction of self-consistent fields differ in the way the interaction is averaged. The procedure to do the self-consistent calculation is: one first makes a trial guess for the wave functions of all electrons and calculate its effective Kohn-Sham potential, V_{KS}. With this effective potential the Kohn-Sham equation is solved to get a new wavefunction. From these, a new V_{KS} is calculated, and so on. Self-consistency is achieved at this point, meaning that the wave function and the effective potential are self-consistent with each other, that is the wave functions correspond to those obtained by solving the Schrödinger equations with this potential. The PWscf method implements both Norm-conserving (NC) and Ultrasoft (US) pseudopotentials.

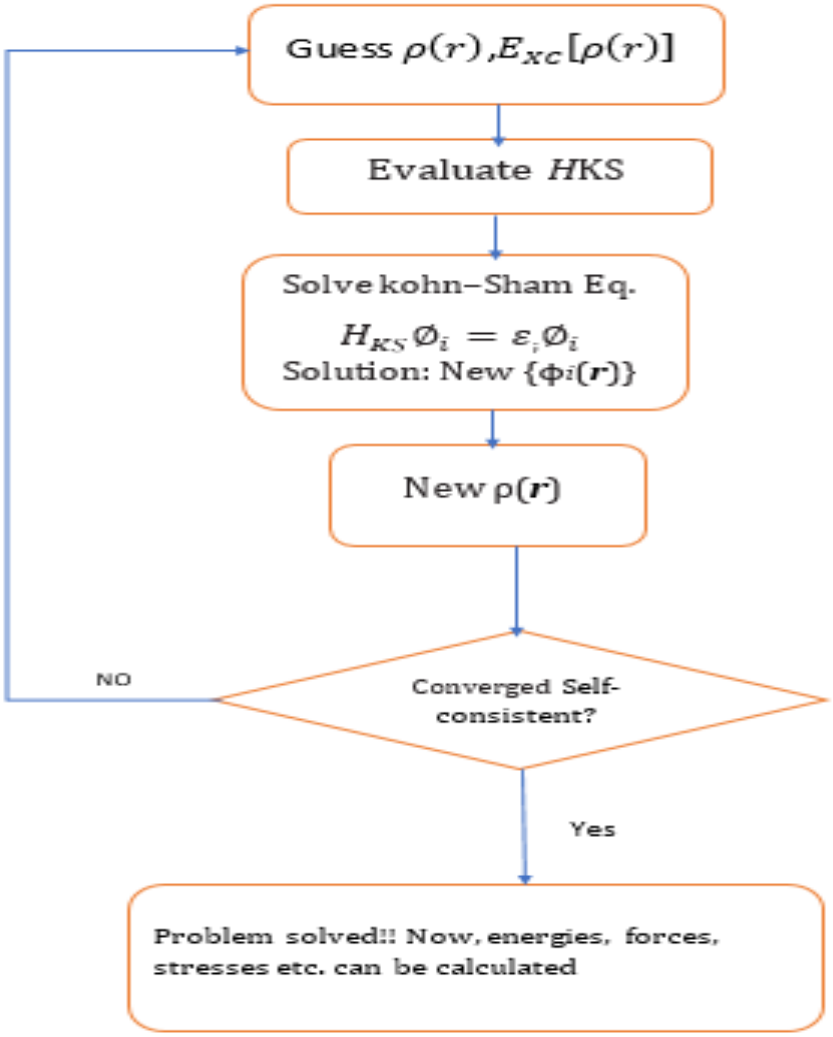

Figure 8. Calculation of the Kohn-Sham ground state

4 Results and Discussion

To study the properties of JTMDs and WS_2 monolayer heterostructures, it is necessary to study the geometric and electronic properties of each JTMDS and WS_2 monolayers.

4.1 Computational Details

Band structure and DOS of WS_2 and JTMDs monolayers and electronic proprieties of different heterostructures have been calculated. Besides, the lattice parameters, band alignment, and average electronic potential difference of the heterostructures have been calculated. All calculations have been performed under the framework of DFT as implemented in Quantum ESPRESSO using pseudopotentials taken from Quantum ESPRESSO homepage and VASP. For all cases the pseudopotentials are of the form of generalized-gradient approximation developed by PBE. Ultrasoft pseudopotentials (US) were used when performing DFT calculations on the TMDCs and heterostructures. The method used for calculations of band structure and material parameters involves twosteps, self-consistent and actual calculations. The first thing that has been done is to decide the appropriate values (convergence test) for the cutoff energy, lattice parameter, and the Brillouin zone sampling. This has been done by varying the parameters and performing self-consistent calculations in order to get a converged minimum total energy. After this, the structure is 'relaxed' for geometric optimization since we do not need to move our atom at Z-axis (it is kept as a vacuum). The calculations were performed according to Figure 10.

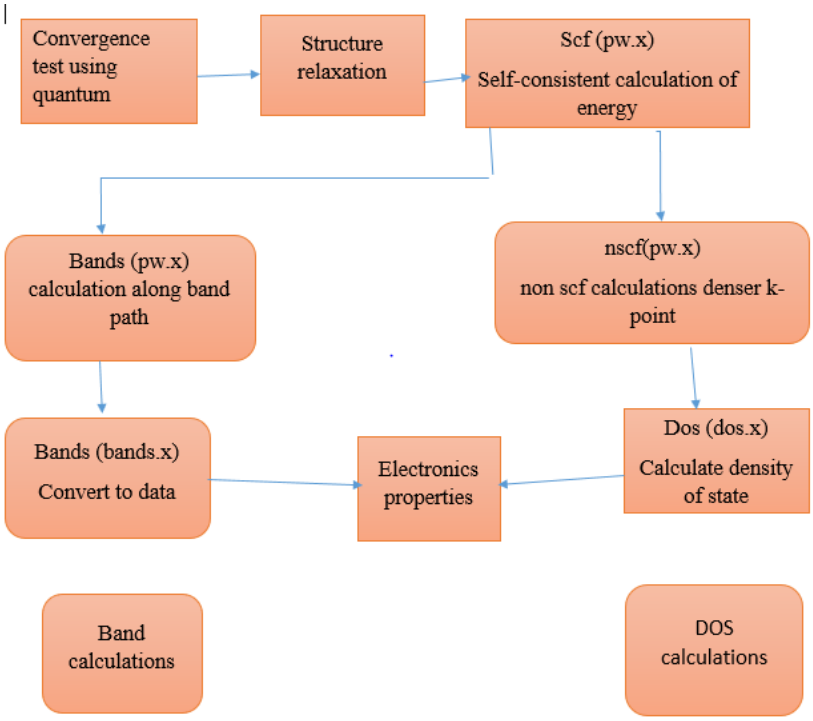

Figure 9. Methodology followed in Quantum-ESPRESSO and VASP to calculate properties of the material.

All DFT calculations were performed with the Quantum-ESPRESSO Simulation Package and VASP. The electronic exchange–correlation energy was treated using the GGA-PBE [44],[45],[46]. A kinetic cutoff energy of 60Ry with ecutrho 600Ry (10 * ecutwfc) was used for the plane-wave expansion set. The **k**-point sampling in the Brillouin zone was implemented using the Monkhorst–Pack scheme with the grid 12 12 1 for the WS_2, JTMDs monolayers and the heterostructures. A vacuum layer of 15Å along z-axis is added to interrupt the artifacts of the periodic boundary conditions. The interfacial interactions of WS_2 and JTMDs heterostructures were treated by using the PBE functional with the vdW correction (DFT-D3)[47]. 3X3X1 supercell was used to build bilayer heterostructure that expand the structural constraints.

4.2 Convergence Tests

To determine the basic parameters, we have carried out different self-consistent field calculations (scf) for the kinetic energy cut-off, K-points grid, and charge density cutoff (ecutrho) for testing the convergence of total energy with each parameters and lattice optimization calculation to get the minimum energy.

4.2.1 K-point grid

Large number of K-points are important to perform the Brillouin zone interaction in discrete scheme. The rectangular grid points of dimensions Kx×Ky×Kz, spaced evenly throughout the Brillouin zone is called k-points grid. Accurate results can be obtained by taking more grid points; however, it is computationally expensive. First, scf calculations were performed, total energy with different values of k-point grids starting from 1×1×1 to 18×18×1.

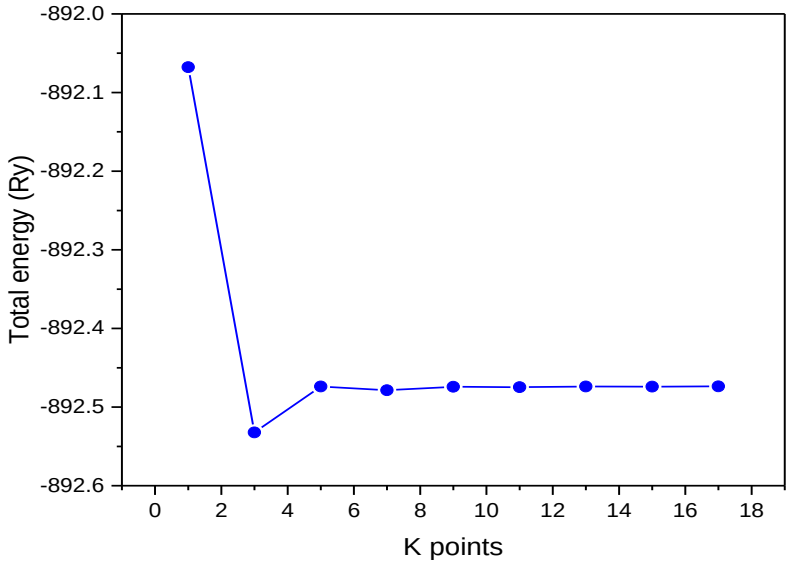

Figure 10.Total energy Vs k-point grid of monolayer WS_2

Figure 10. Shows that the total energy starts to converge from 5x5x1, so it is appropriate to use k-points 12x12x1 for further calculations in order to get accurate results.

4.2.2 Kinetic Energy cut-off (ecutwfc)

Kinetic energy cut-off is the neighboring interaction in the periodic system. If we take large cut-off energy, we include long range interactions and the results will be more accurate, but this takes more computing resources.

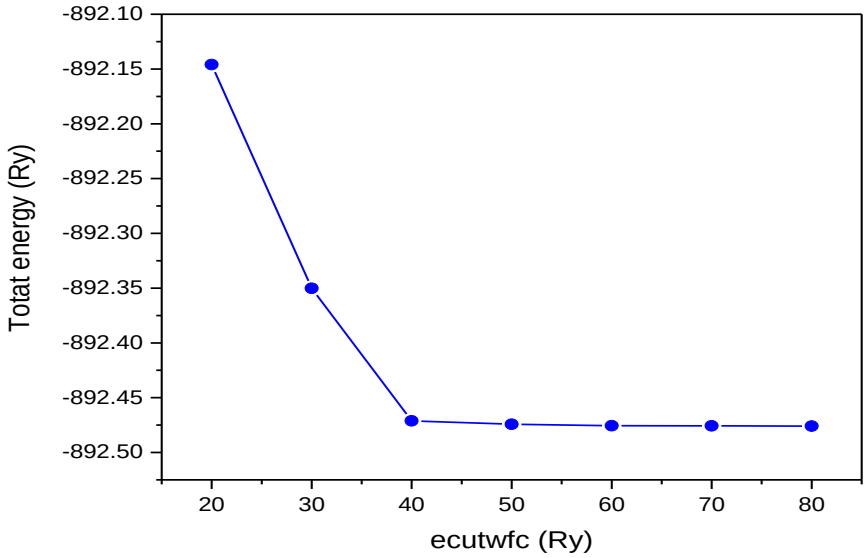

Figure 11.Total energy Vs kinetic energy (ecutwfc)

Figure 11. Shows the calculated total energy for different plane waves cutoff (ecutwfc) from 20Ry up to 80Ry. Convergence of total energy of the system is shown starting from 50Ry ecutwfc, so 60Ry ecutwfc was used in the rest of the calculations.

4.2.3 Charge density

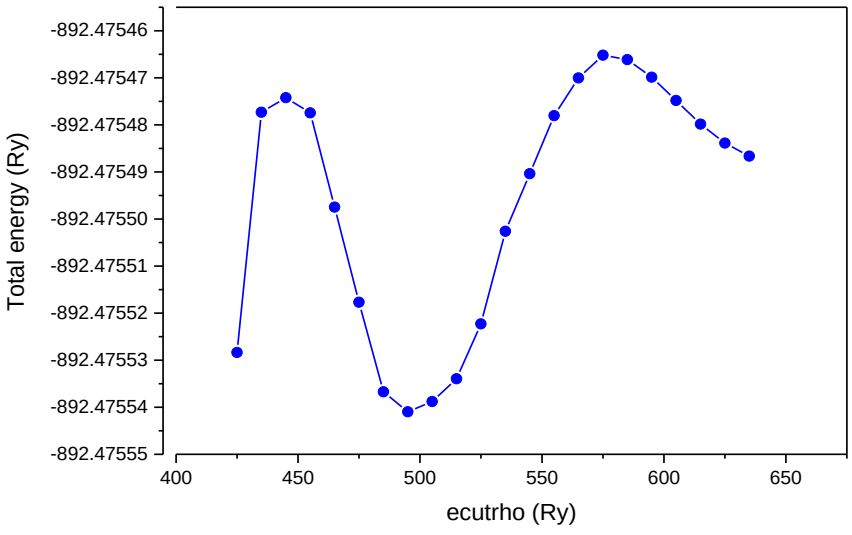

Figure 12. Total energy Vs charge density

It can be seen from Figure 12 the convergence of total energy is achieved starting approximately from 580Ry charge density. Ecutrho is a multiple of ecutwfc and with the suggested values of ecutwfc=60 and ecutrho=580, the multiplication factor is nearly 10. For convenience, multiple of 10 for ecutwfc was taken and the ecutrho value becomes 600 Ry.

4.2.4 Lattice Parameter

The equilibrium parameter is the one that has the minimum energy from the curvature of the total energy vs lattice parameter graph. The calculated total energy versus lattice parameter of WS_2 monolayer in the range of 3.14 Å to 3.22Å is depicted in Figure 13.

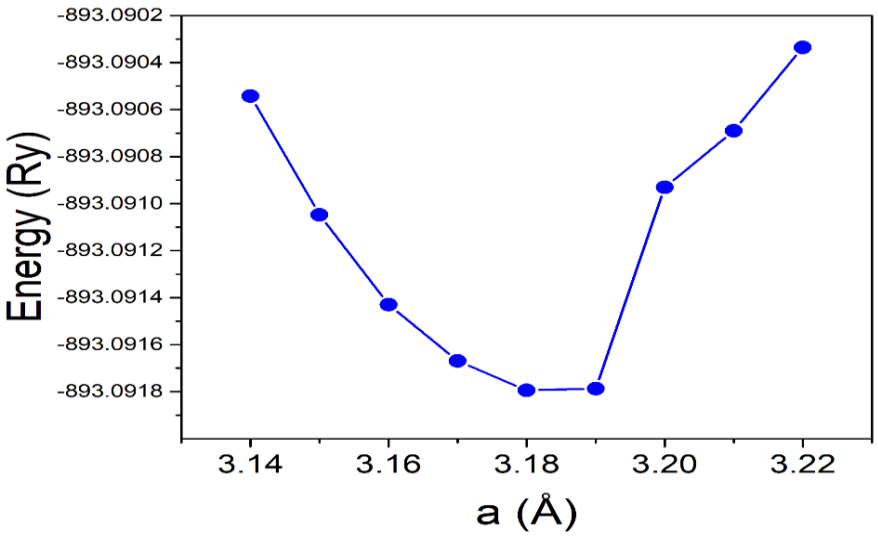

Figure 13. Total energy vs lattice parameter

Figure 13. Shows that the equilibrium lattice parameter is 3.18 **Å** and so this is the minimum distance between atoms in monolayer WS_2, hence, it is the value that yields the lowest total energy.

4.3 Optimized Structures of JTMDs Monolayers

To find out the most stable structure of each JTMDs monolayers, firstly the structures were optimized by using PBE methods. The optimized lattice constants are summarized in Table:3. These results agree very well with previous works. In addition, the lattice mismatch between JTMDs and WS_2 monolayers were calculated and are presented in Table 3.

Table 3: Optimized lattice parameter and lattice mismatch

MXY	Current work Lattice a(Å)	Reference Lattice a(Å)	Lattice mismatch (%)
MoSSe	3.25	3.24[7], 3.25[23]	2.154
MoSTe	3.35	3.35[7], 3.32[48]	5.075
MoSeTe	3.42	3.42[7], 3.405[49]	7.018
WSSe	3.25	3.23[7], 3.247[50]	2.154
WSeTe	3.54	3.42[7], 3.45 [51]	10.170
WSTe	3.38	3.34[7], 3.37[52]	5.917
WS_2	3.18	3.181[19], 3.19[53]	

Lattice matching, one type of 2D on the other one to form heterostructures coupled with weak vdW interaction, are of interest in 2D electronic and optoelectronics technology due to their atomically sharp interface, minimal trap states, and absence of dangling bond[54].

Matching lattice constants of MoSSe, MoSTe and WSSe (lattice mismatch about 2.154% to 5.075%) are desirable to form heterostructures with WS_2. Lattice match (or a very small mismatch) between two adjacent semiconductor materials minimizes dangling bonds. Therefore, 3x3 unit cells of monolayer JTMDs and WS_2 were used to create the heterostructures.

Due to similar lattice constants of MoSSe, MoSTe and WSSe with WS_2 a new 2D heterostructures of MXY/WS_2 composed of JTMDs (MoSSe or MoSTe or WSSe) and WS_2 monolayers were designed through first principle calculations. The geometry structure, electronic properties, and band alignments were systematically investigated from a theoretical point of view.

4.4 Electronic Property of WS_2 and JTMDs Monolayers

Electronic band structure and partial density of states (PDOS) of these monolayers were calculated. The electronic band structures ofWS_2, WSSe, MoSSe, and MoSTe monolayers are shown in the Figure 14. Direct bandgap was observed for WS_2, WSSe and MoSSe and an indirect bandgap was exhibited for MoSTe monolayer with the bandgap values ~ 1.82 eV, 1.71 eV, 1.56 eV, and 1.01 eV for WS_2, Janus WSSe, MoSSe, and MoSTe monolayers, respectively, using GGA-PBE. These

values are consistent with previous reports computed by considering the GGA-PBE exchange correlation function[55], [56], [57], [58], [59].

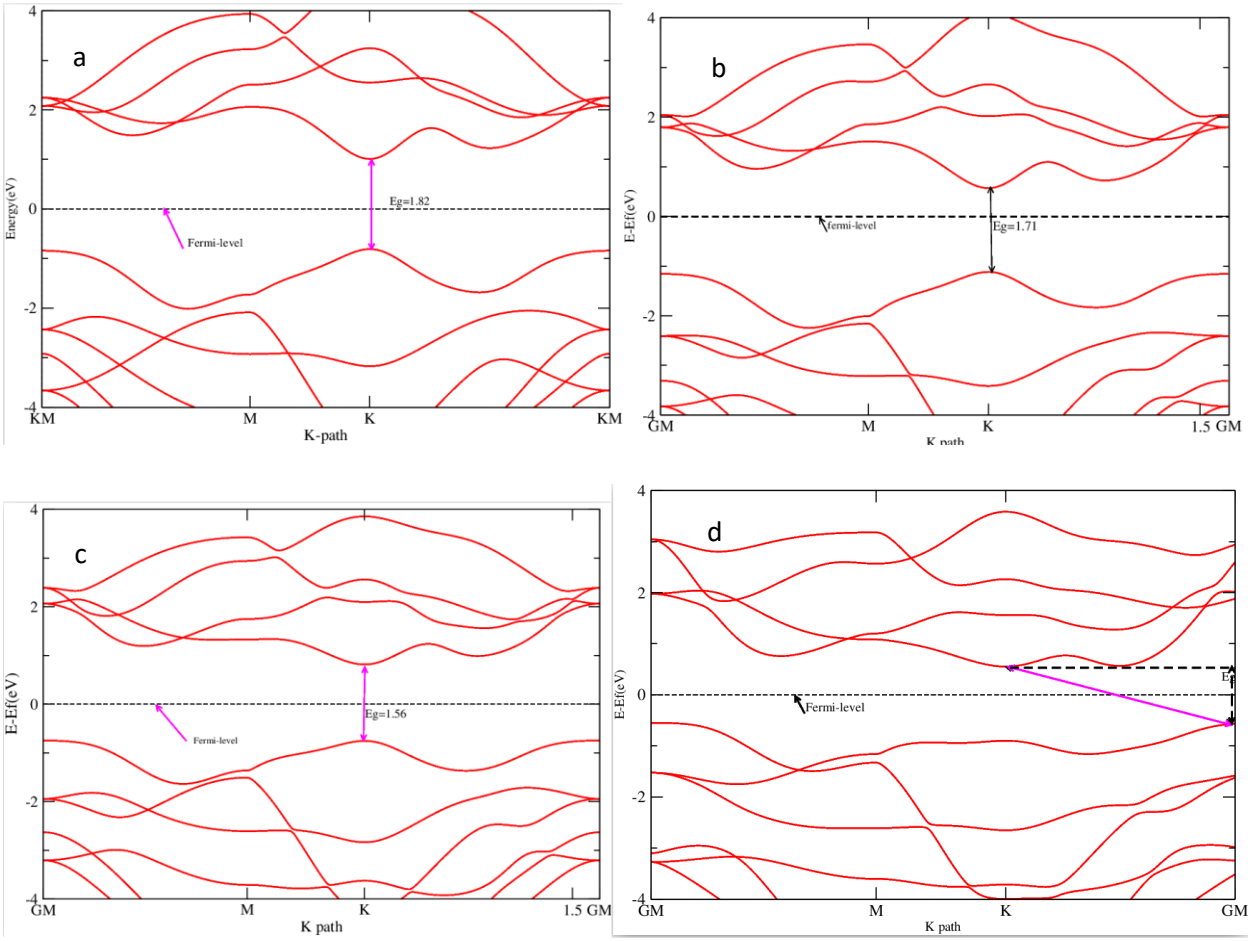

Figure 14. Electronic band structure of (a) WS_2, (b) WSSe, (c) MoSSe, and (d) MoSTe monolayers with high symmetry k-path using GGA-PBE

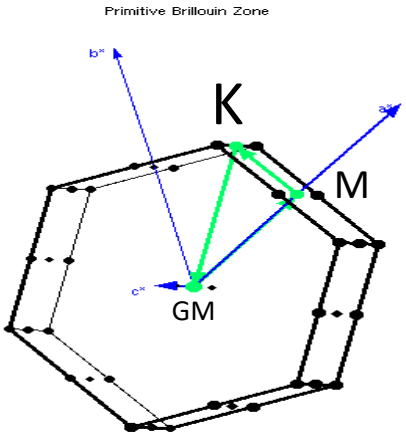

Figure 15. High symmetry path for monolayer

PDOS were computed for WS_2, Janus WSSe, MoSSe, and MoSTe monolayers in the range of -16 to 4 eV and results are summarized in Figure5-8. The total and PDOS of WS_2 originates from W-5d, S-2p, W-3,4p, S-1s and W-1,2s states and the S-2p and W-5d were the dominant states. The upper valence band (located between– 8.0 eV to ~0 eV) is mainly made up of W-5d and S-2p states and it is dominated by S-2p states. In the conduction band, the W-5d plays the dominant role from 0 to 4.5 eV and the region from 4.5 to 8.0 eV consists of W-1,2s, W-3,4p and S-2p states. The contribution far from the Fermi energy is mostly dominated by W-3,4p and W-1,2s from 4.5eV to 8eV in WS_2 monolayer. Similarly, near to the fermi level, Janus WSSe monolayer is mostly dominated by the W-5d, Se-p and S-p orbitals and states far from Fermi energy are mainly from S-s and Se-s. A similar contribution is observed for MoSSe, where CBM is dominated by Mo-4d, S-2p and Se-2p orbitals and states in VBM are also dominated by Mo-4d, S-2p, and Se-2p orbitals. For MoSTe near to the fermi level, Mo-4d has the highest contribution. These values are in agreement with the previous reports[7].

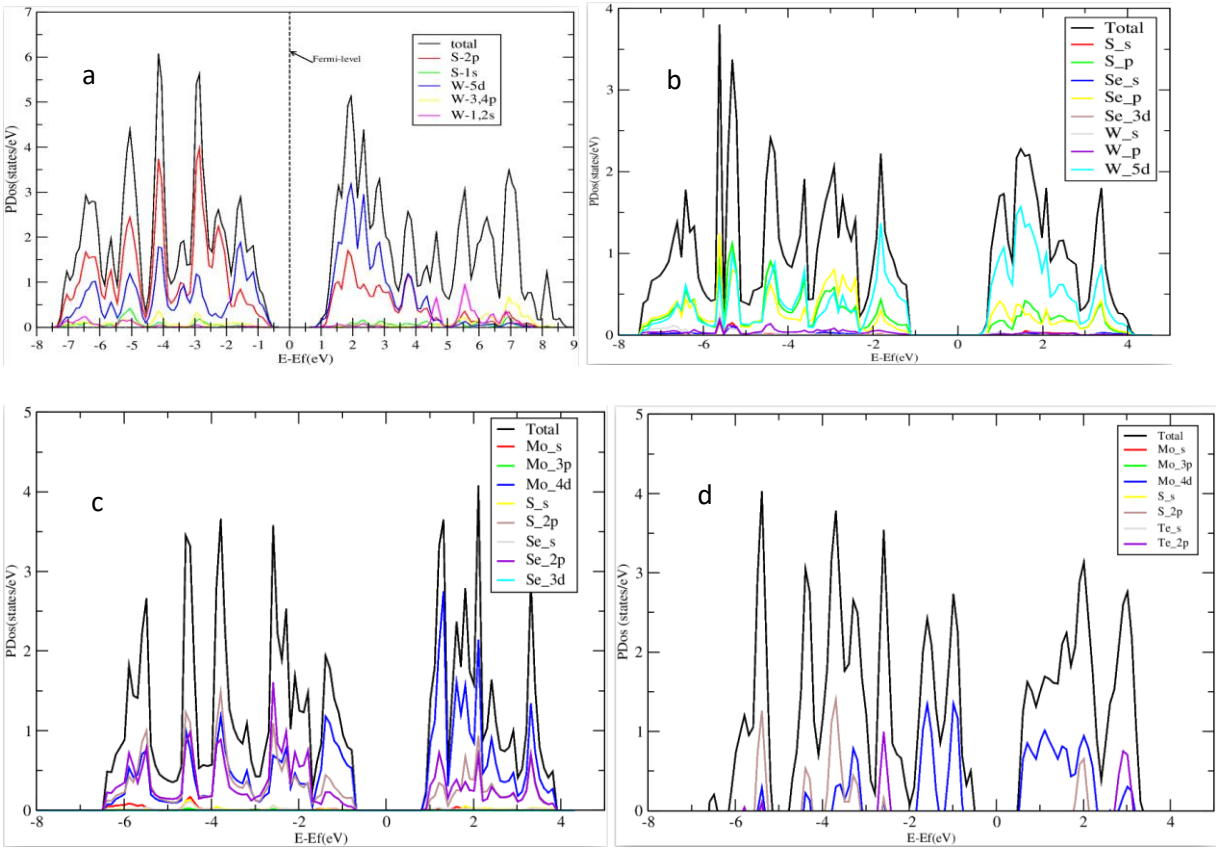

Figure 16.Partial density of states of(a) WS_2, (b) WSSe, (c) MoSSe and (d) MoSTe monolayers

4.5 JTMD/WS_2 Monolayer Heterostructures

Owing to the facts that Janus monolayers MoSSe, WSSe, MoSTe and WS_2 have the same crystal structure and the lattice mismatch is less than 5.075%, as shown in Table 3. WS_2 monolayer was used to construct the heterostructures with Janus monolayer of MoSSe, WSSe and MoSTe.

4.5.1 Optimized Structures of Heterostructures

To find out the most stable structure of each four main stacking patterns of the heterostructures, the structures were firstly optimized by using GGA-PBE methods. The optimized lattice constants by GGA-PBE methods are summarized in Table 4. To find a stable configuration for the $MoSSe/WS_2$, $WSSe/WS_2$ and $MoSTe/WS_2$ heterostructures, four stacking configurations were considered.

Table 4: Stacking configurations of JTMDs/WS_2 Heterostructures

Configuration(pattern)	$MoSSe/WS_2$	$WSSe/WS_2$	$MoSTe/WS_2$
Config_AA a(Å)	3.215	3.215	3.345
Config_AB a(Å)	3.235	3.235	3.345
Config_AC a(Å)	3.235	3.235	3.345
Config_AD a(Å)	3.215	3.215	3.305

After geometry optimization calculations, the most stable configuration is the one with the most negative binding energy and the suitable interlayer distance. In $MoSSe/WS_2$ configuration (AA), the atoms of Janus monolayer MoSSe located above the S atoms of WS_2 and the Se atoms of the Janus monolayer MoSSe on top of the Mo atoms of MoSSe. In the case of AB-configuration, the atoms of Janus monolayer MoSSe above the S atoms of WS_2 and the Se atoms of the Janus MoSSe monolayer located below the Mo atoms of MoSSe. In AC, the Se atoms of Janus monolayer MoSSe above the Mo atoms of MoSSe and the W atoms of the WS_2 monolayer centered above the MoSSe hexagon. In the last configuration (AD), the Se atoms of Janus monolayer MoSSe located below the Mo atoms of MoSSe and the W atoms of monolayer WS_2 are centered below the Janus monolayer MoSSe hexagon. To determine the stability, the binding energy (E_b) per unit cell was calculated using the following formula:

$$E_b = E_{heterostructure} - E_{monolayer1} - E_{monolayer2} \quad (5.1)$$

where $E_{heterostructure}$ is the total energy of the heterostructures and $E_{monolayer1}$ and $E_{monolayer2}$ are the total energy of the JTMDs and WS_2 monolayers, respectively. Figure 17 shows the four main stacking patterns (bottom and side view)

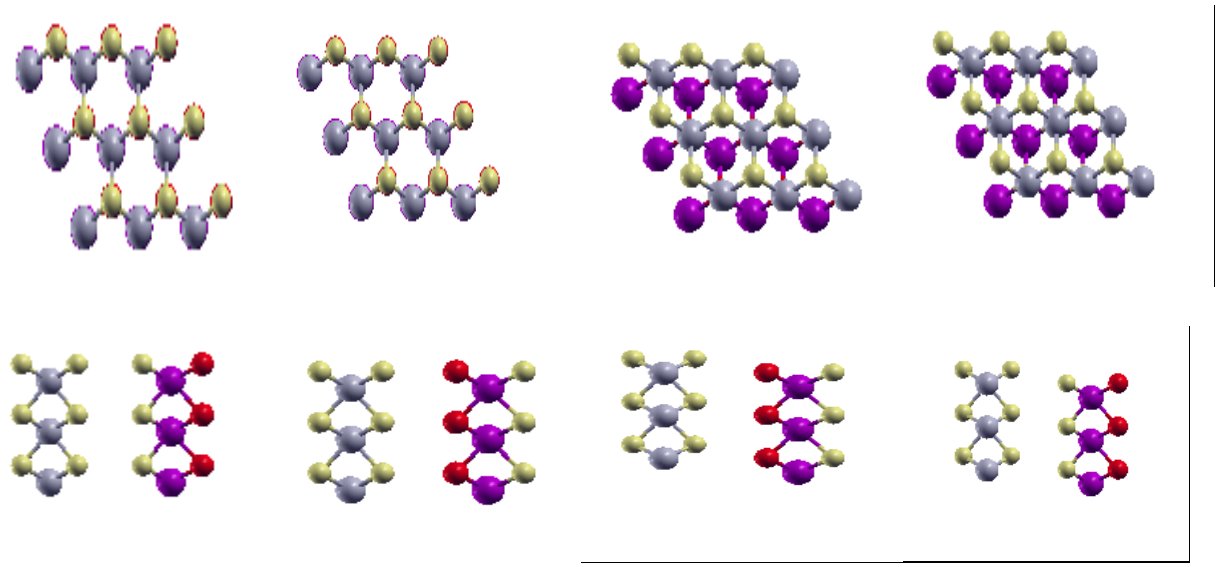

(a) **(b)** **(c)** **(d)**

Figure 17. Different stacking patterns (a), (b), (c) and (d) for configurations_AA, AB, AC and AD respectively.

where Mo, S, Se or Te and W

The binding energy and interlayer distance of MoSSe, WSSe, and MoSTe on the WS_2 monolayer of the heterostructures are listed in Table 5. According to the definition of E_b, a more negative value of E_b indicates that the interfaces between these two single layers are more energetically stable and could be easier to obtain such structures experimentally[51]. As it is listed in Table 5, the calculated results show that differences in E_b between the different configurations, which indicates that the stacking pattern show a significant influence in the total energy of the heterostructures. To examine the optimum structural stabilities of the heterostructures, the binding energies of the heterobilayer systems are calculated, as shown in Table 5.

To better understand the properties of JTMDs/WS_2 heterostructures, four stacking pattern models including the binding energy E_b (Ry) and the interlayer distance D(Å) were calculated.

Table 5:Binding energy and interlayer distance for different stacking pattern of the heterostructures

Configuration		MoSSe/WS_2	WSSe/WS_2	MoSTe/WS_2
CONFIGURATION-AA	E_b	-0.00791305	-0.01127792	0.02088135
d		3.6404	3.5659	
CONFIGURATION-AB	Eb	-0.00904175	-0.01190461	0.00169084
d		3.6907	3.6313	
CONFIGURATION-AC	Eb	-0.0150775	-0.01917887	-0.00572721
d		3.6196	3.5715	3.7456
CONFIGURATION-AD	Eb	-0.01344856	-0.01847481	-0.00599605
d		3.5293	3.4678	3.5133

Table 5 shows, the values of E_b demonstrate that Configuration-AC and AD have a lower binding energy than Configuration-AA and AB for each heterostructures, thus configuration-AC and AD are much more energetically stable than the two configurations. The two configurations, AA and AB, of MoSTe/WS_2 show positive binding energy implying difficulty in forming heterobilayer from MoSTe and WS_2. The negative binding energy in the JTMDs/WS_2 heterostructures is good indicator of weak vdW forces that bound JTMDs with WS_2 monolayer.

4.5.2 Properties

The electrical properties of JTMDs monolayers and JTMDs/WS_2 heterostructures for each configuration calculated by GGA-PBE is presented in Table 6.

Table 6: Electrical properties of JTMDs monolayers and JTMDs/WS_2 heterostructures using GGA-PBE.

MXY or MXY/WS_2	BANDGAP [eV]	Fermi level [eV]	Electron affinity [eV]	Work function [eV]
WS_2	1.82	0.724	3.9[53]	4.91
MoSSe	1.56	0.787		4.895
WSSe	1.71	1.517		4.310
MoSTe	1.01	0.988		4.557
MoSTe_WS_2				
Config _AC	0.513(Ind)	1.198	-5.372	5.756
Config _AD	0.5324(Ind)	1.951	-4.412	4.633
WSSe_WS_2				
Config _AC	1.076(Dir)	0.380	-4.552	5.458
Config _AD	1.254(Ind)	0.58	-3.903	5.064
MoSSe_WS_2				
Config _AC,	1.23(Ind)	0.578	-4.583	5.619
Config _AD	1.093(Ind)	1.016	-4.089	4.963

Figure 18 shows the plane-averaged electrostatic potential of JTMDs/WS_2 heterostructures for each configuration. The highest points in the Y-direction gives the value of averaged electrostatic potential. The electrostatic potential difference between the Janus MoSSe/WS_2, MoSTe/WS_2 and WSSe/WS_2 monolayers are calculated to be 5 eV, 10 eV and 5 eV, respectively.

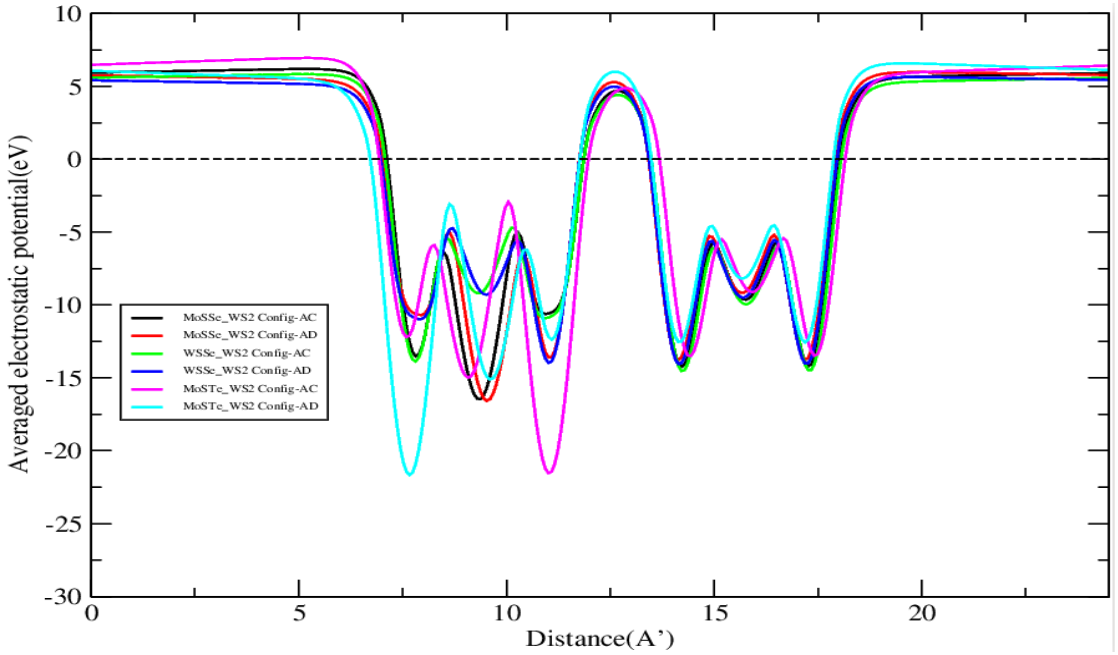

Figure 18. Plane-averaged electrostatic potential of JTMDs/WS_2 heterostructures for different configurations.

The JTMDs/WS_2 heterostructure electronic band structures for different configurations along with the monolayers WS_2 and Janus TMDCs are investigated and demonstrated in Figure 20 to 22. The projected band structures of the MoSSe/WS_2 heterostructure configuration-AC is shown in Figure 20(a). It can be clearly seen that the VBM at gamma point is contributed from Mo of MoSSe monolayer while its CBM at K point is contributed from W of WS_2. Similarly, the projected band structures of the MoSSe/WS_2 heterostructure configuration-AD is shown in Figure 20(b), the VBM at gamma point is contributed from W of WS_2 monolayer while its CBM at K point is from Mo of MoSSe.

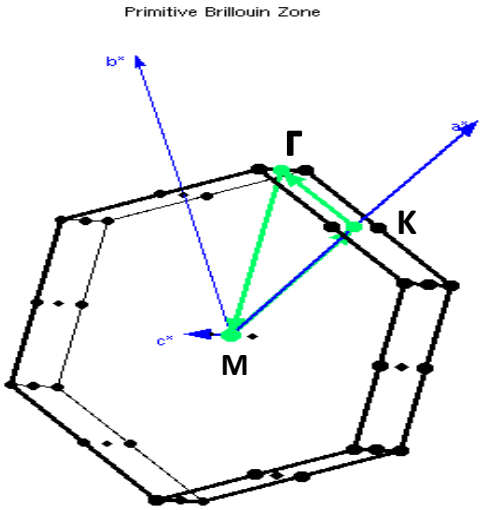

Figure 19.High symmetry path for heterostructures

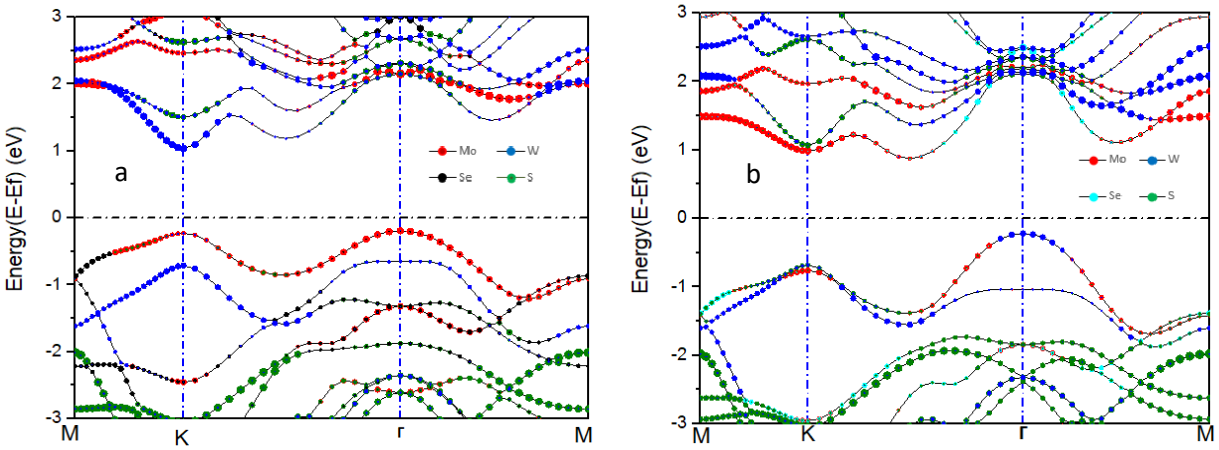

Figure 20. Band structure of MoSSe/WS_2 heterostructure (a) configuration-AC and (b) configuration-AD.

The projected band structures of the $WSSe/WS_2$ heterostructures for configuration-AC and AD are shown in Figure 21(a) and (b). Both the CBM and the VBM of the $WSSe/WS_2$ heterostructure for configuration-AC are located directly at the Dirac K point. W of WS_2 or WSSe contributes for the CBM and VBM (it was difficult to identify which monolayer contributed for VBM and CBM and needs additional calculations as shown on Figure 21(a). However, for configuration-AD, it is clearly seen that the VBM at Gamma point is contributed from W of WS_2 or WSSe and CBM at K point is from W of WS_2 or WSSe as shown in Figure 21(b).

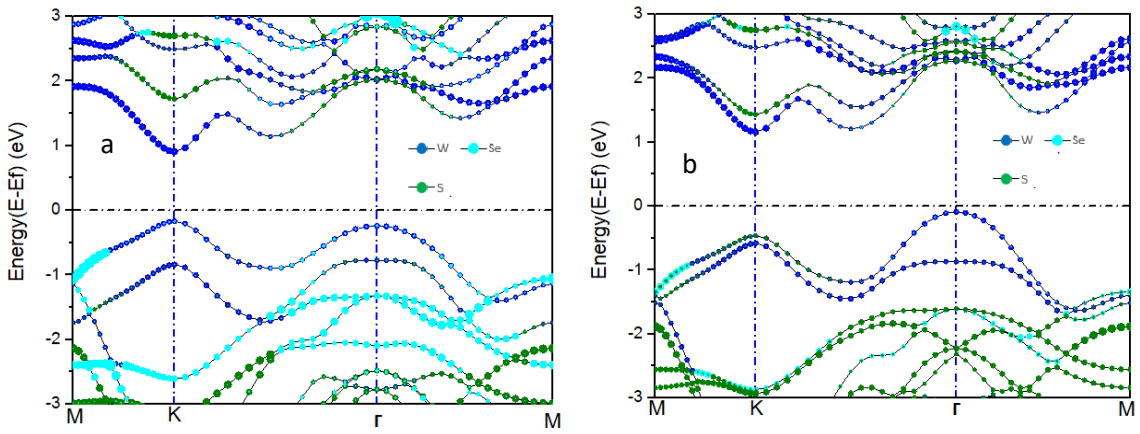

Figure 21. Band structure of $WSSe/WS_2$ heterostructure (a) configuration-AC and (b) configuration-AD

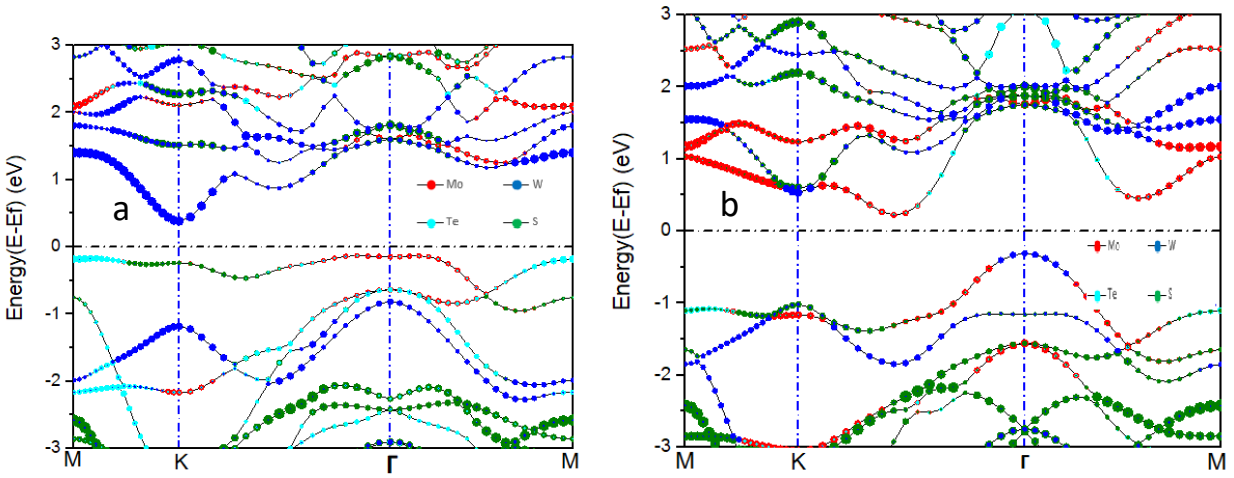

Figure 22. Band structure of $MoSTe/WS_2$ heterostructure (a) configuration-AC and (b) configuration-AD

The projected band structure of $MoSTe/WS_2$ heterostructure configuration-AC is shown in Figure 22(a). The VBM at Gamma point is contributed from Mo of MoSTe monolayer while its CBM at K point is contributed from W of WS_2. The projected band structures of the $MoSTe/WS_2$ heterostructure configurations-AD is shown in Figure 22(b). The VBM at Gamma point is contributed from W of WS_2 monolayer while its CBM is located at the K-Γ path is from Mo of MoSTe.

To further investigate the electronic structure and describe interlayer interactions between monolayer MoSSe, WSSe, MoSTe with WS_2, the TDOS and PDOS for heterostructures are presented in Figure 23 to 25. The states of $MoSSe/WS_2$ around the Fermi level are mostly formed by Mo-d, S-p, Se-p and W-d orbitals. The CBM of the $MoSSe/WS_2$ heterostructures are contributed primarily by Mo-d, S-p, Se-p and W-d orbitals from Mo, S, Se and W atoms, respectively, while the main contribution comes from Mo-d, S-p, Se-p and W-d orbitals for its VBM.

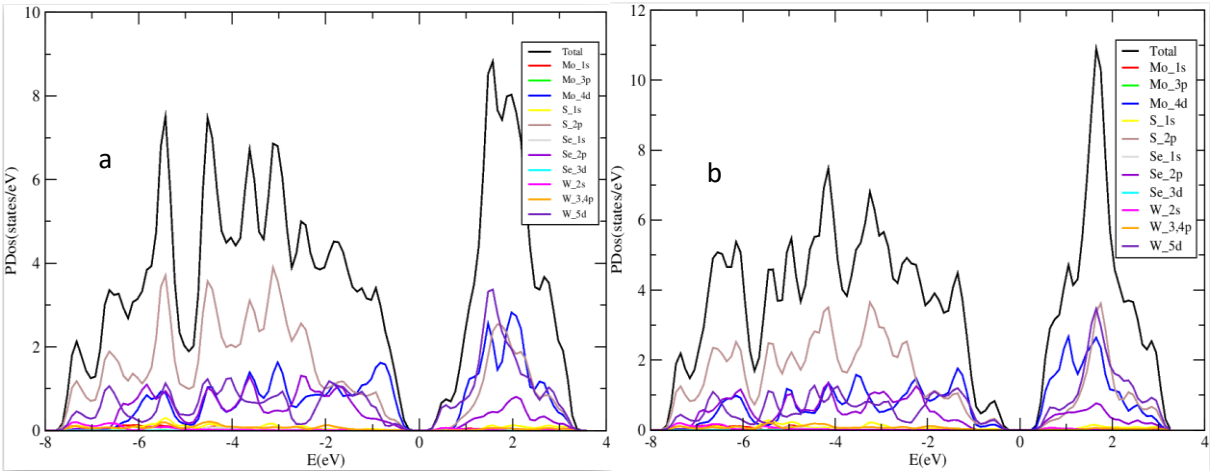

Figure 23. TDOS and PDOS of $MoSSe/WS_2$ monolayer (a) configuration-AC and (b) configuration-AD.

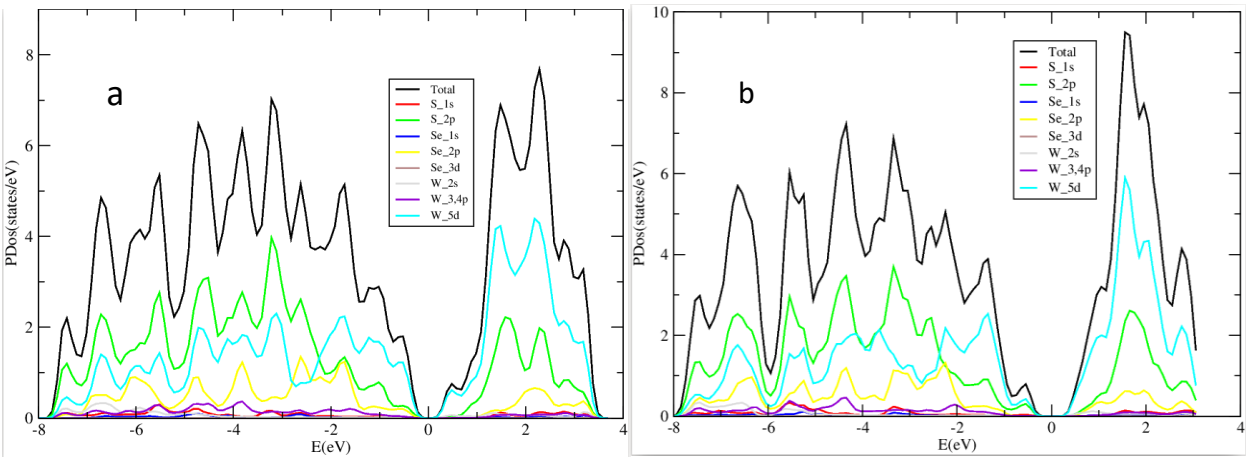

Figure 24. TDOS and PDOS of $WSSe/WS_2$ monolayer (a) configuration-AC and (b) configuration-AD.

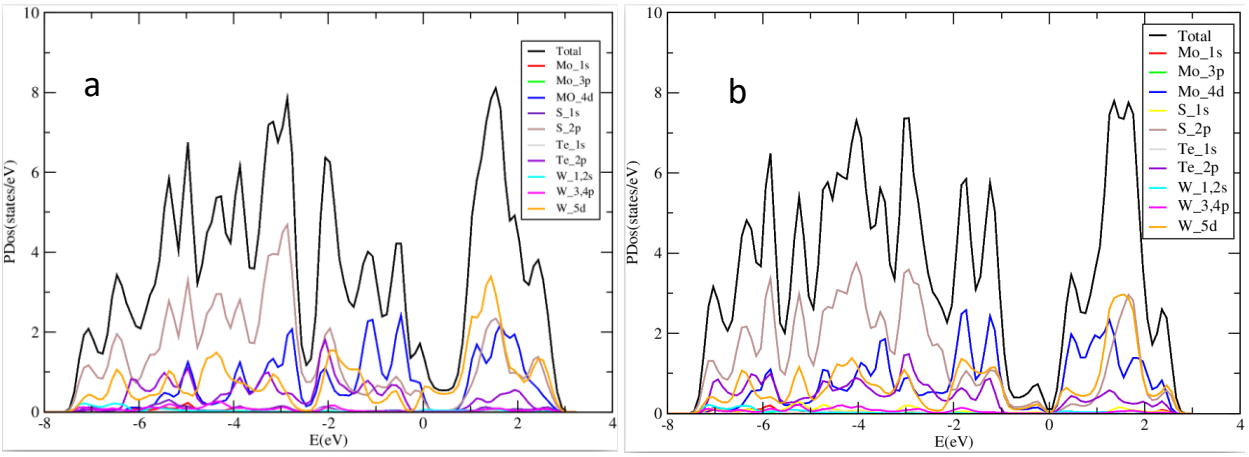

Figure 25. TDOS and PDOS of $MoSTe/WS_2$ monolayer (a) configuration-AC and (b) configuration-AD.

In Janus $MoSSe/WS_2$ and $MoSTe/WS_2$ heterostructures, the CBM of configuration-AC are localized on the WS_2 and VBM on the MoSSe and MoSTe, respectively. While for configuration-AD, the CBM are localized on the MoSSe and MoSTe and the VBM on the WS_2, showing all are of type-II band alignment for configuration-AC and AD that separates free electrons and holes spontaneously[60]. It is known that the majority of photovoltaic devices need the electronic structure of type-II band alignment to improve the photoelectric conversion efficiency. The predicted $MoSSe/WS_2$ and $WSSe/WS_2$ vdW heterostructures have direct and indirect bandgap of (~1.1, 1.23 eV) and (1.08, 1.25 eV), respectively, with configuration-(AC, AD) as shown in the Table 6. Such bandgap values are similar to that of bulk silicon (~1.16 eV), which is optima for

photovoltaic application in solar cells. Conversely, $MoSTe/WS_2$ heterobilayer possess too small bandgap to efficiently harvest the visible light portion of the sun spectrum. Further study is needed to modulate the bandgap by doping with other heavy elements to create stress in the structure and increase the bandgap.

Migration of photogenerated electrons and holes in the $MoSSe/WS_2$ and $MoSTe/WS_2$ heterostructures, that is between the MoSSe (or MoSTe) and WS_2 layers with configuration-AC and AD, are shown in Figure 26(c), 27(d), 28(c) and 29(c). In the $MoSSe/WS_2$ and $MoSTe/WS_2$ configuration-AC, due to the Conduction Band Offset (CBO) and Valance Band Offset (VBO) of the heterostructures, the photogenerated electrons in MoSSe (or MoSTe) migrated to the CBM of the WS_2 layer, while the photogenerated holes in the WS_2 layer tend to move to the VBM of the MoSSe (or MoSTe). On the other hand, for configuration-AD, the photogenerated electrons in WS_2 migrated to the CBM of the MoSSe (or MoSTe) layer, while the photogenerated holes in the MoSSe (or MoSTe) layer are tend to move to the VBM of the WS_2. Consequently, the band offset of type-II heterostructures such as $MoSSe/WS_2$ can overcome problem associated with the electron-hole recombination.

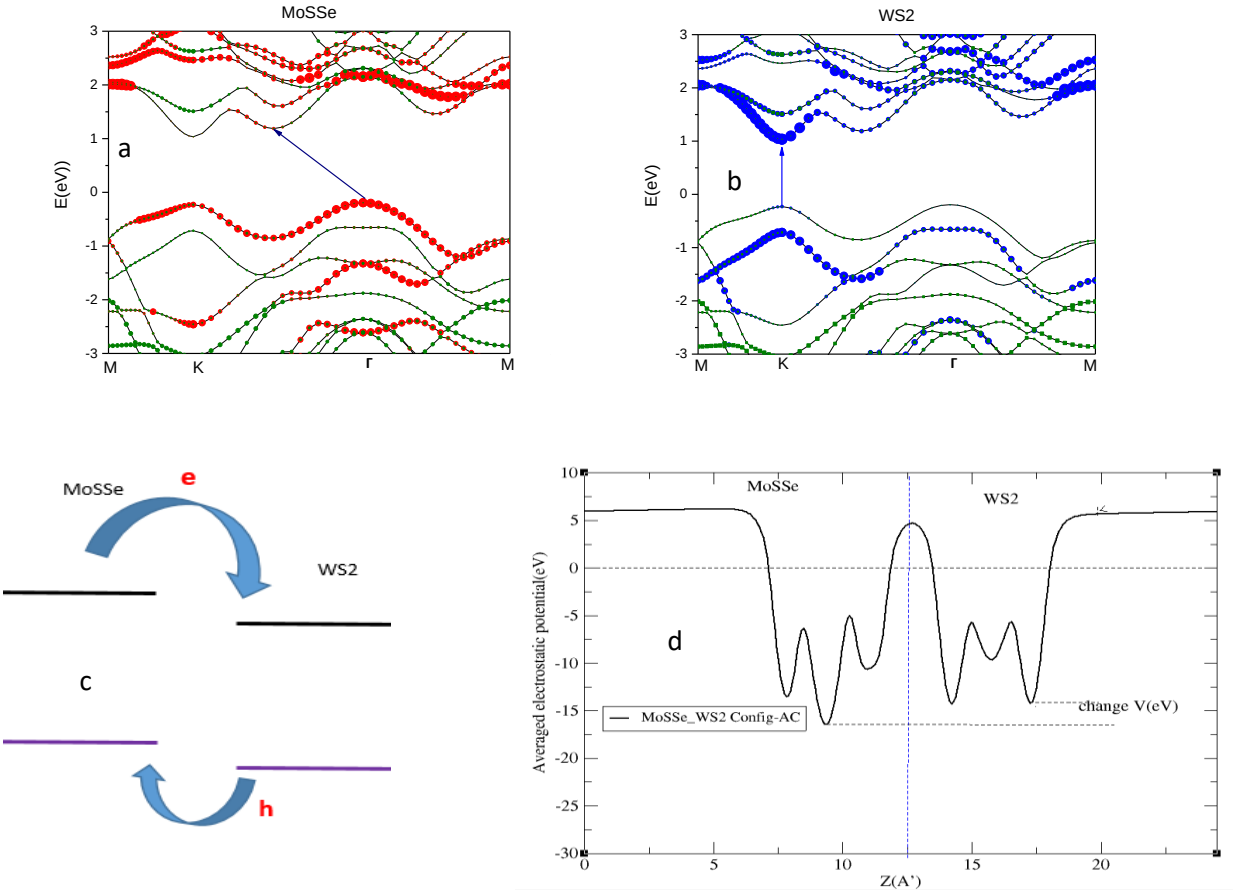

Figure 26(a)Projected band structures of the MoSSe, (b) Projected band structures of the WS_2,(c) Band alignment schematic for migration of photogenerated electrons and holes, and (d) Potential drop across the interface of the MoSSe/WS_2 heterostructure configuration-AC

The built-in electrical field of MoSSe / WS_2 vdW heterostructures also plays an important role in photovoltaic applications since the large built-in electrical field enhances the ability to further enhance the translation of photogenerated charges. Figure 26(d), 27(c), 28(d) and 29(d) show the potential drop in the interface of the heterostructures. The potential drop across the MoSSe/WS_2 and MoSTe/WS_2 vdW heterostructures interface is 5 eV and 10 eV, respectively, which can result in a powerful built-in electric field, and this electric field could induce some effect on the recombination of the photogenerated electron-hole in the heterostructures.

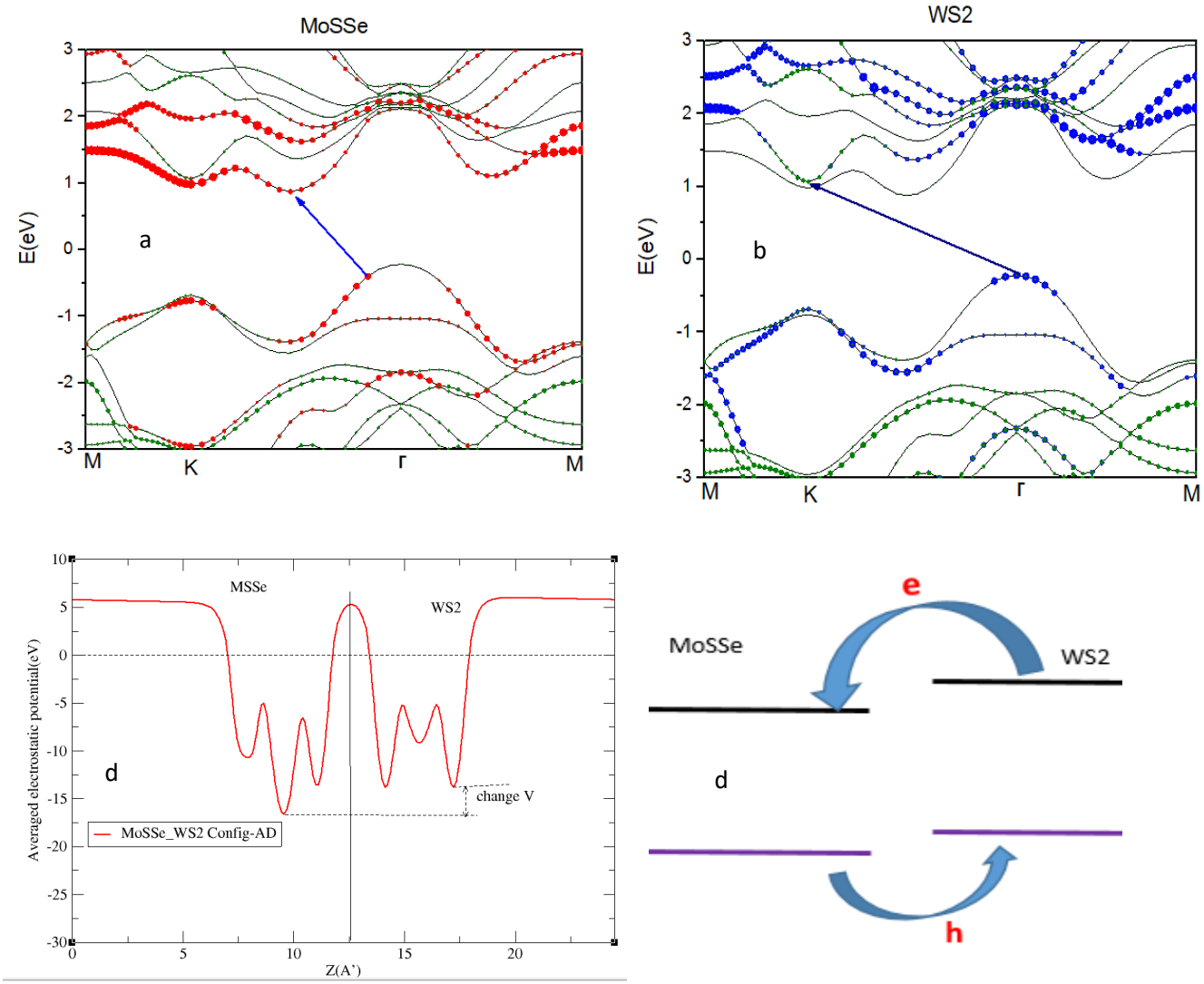

Figure 27: Projected band structures of the MoSSe, (b) Projected band structures of the WS_2, (c)Potential drop across the interface and (d) Band alignment schematic for migration of photogenerated electrons and holes and of the MoSSe/WS_2 heterostructure configuration-AD

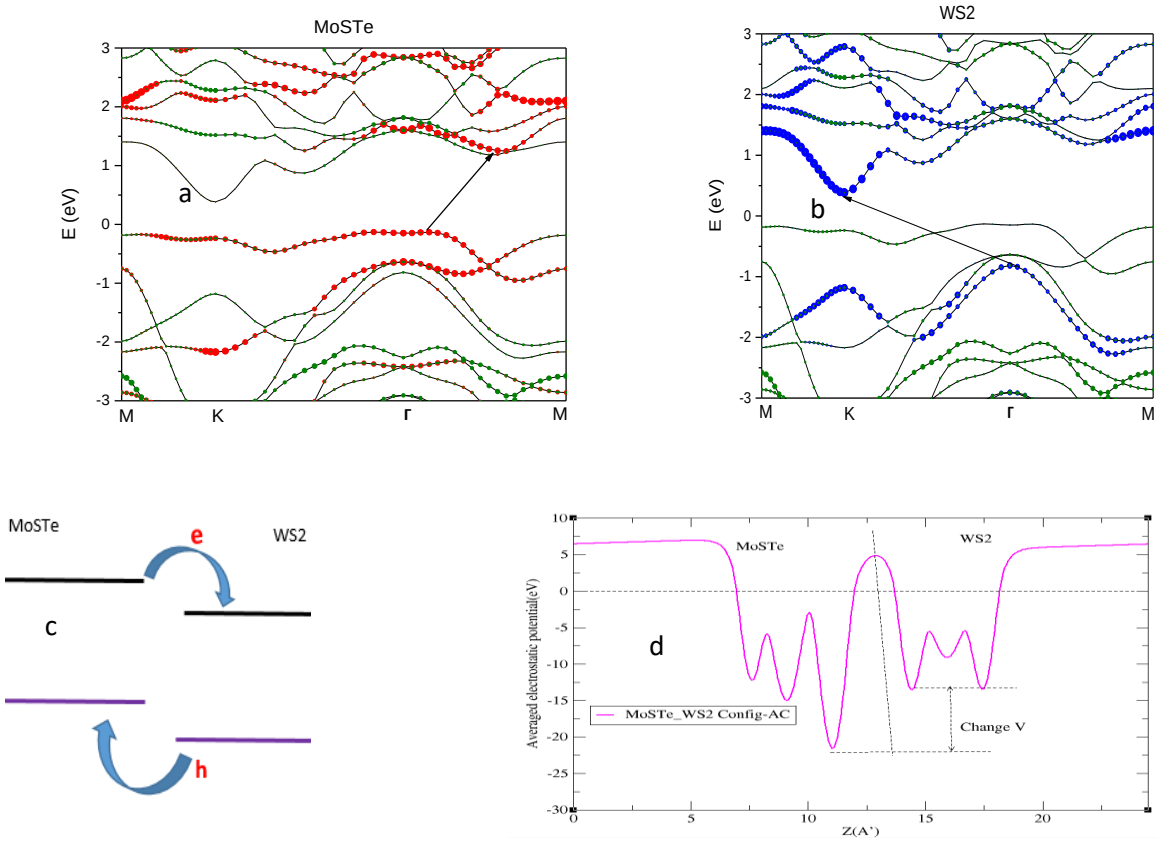

Figure 28 (a)Projected band structures of the MoSTe, (b) Projected band structures of the WS_2, (c) Band alignment schematic for migration of photogenerated electrons and holes and (d)Potential drop across the interface of the MoSTe/WS_2 heterostructure configuration-AC.

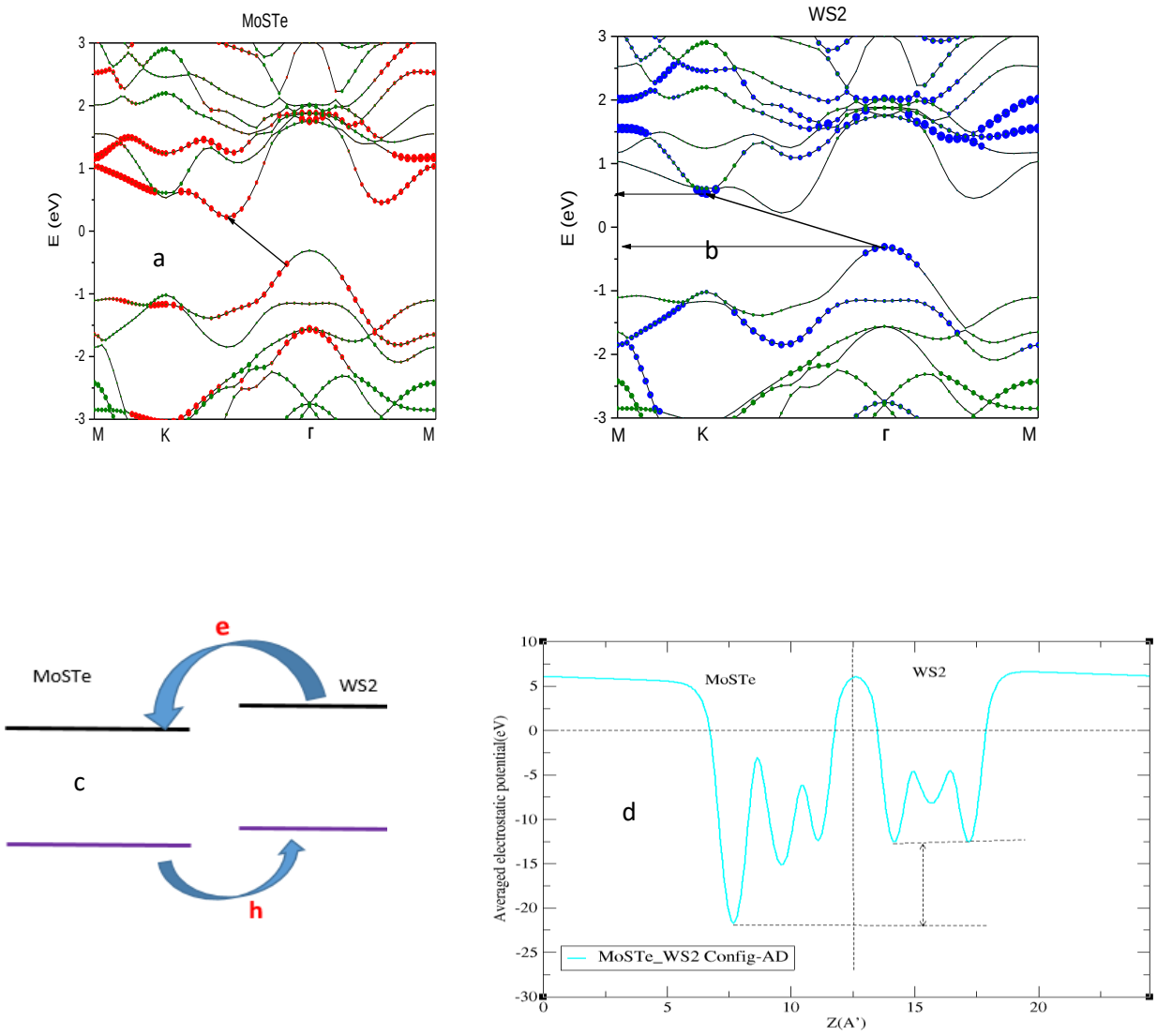

Figure 29(a)Projected band structures of the MoSTe, (b) Projected band structures of the WS_2, (c) Band alignment schematic for migration of photogenerated electrons and holes and (d) Potential drop across the interface of the MoSTe/WS_2 heterostructure configuration-AD.

5 Conclusion and Future Outlook

5.1 Conclusion

In summarize, the structural stability and electronic properties of Janus MoSSe/WS_2, WSSe/WS_2, and MoSTe/WS_2 heterostructures with vdW correction were studied using DFT calculations. Due to the weak vdW interactions, isolated WS_2 and Janus MoSSe, WSSe, and MoSTe monolayers were well maintained in their vdW heterostructure. It was found that the Janus MoSSe/WS_2, WSSe/WS_2 (configuration-AD), and MoSTe/WS_2 vdWs heterostructures are of indirect bandgap while WSSe/WS_2 with configuration-AC is a direct bandgap heterostructure.

The bandgap of the investigated heterostructures are MoSSe/WS_2 (1.23, 1.1 eV), WSSe/WS_2 (1.08,1.25 eV) and MoSTe/WS_2 (0.51, 0.53eV) with configuration- (AC, AD), respectively. The ideal bandgap for achieving the maximum thermodynamically possible conversion efficiency of sunlight to electricity is around 1.3 eV to 2.2 eV. Therefore, except the MoSTe/WS2 heterostructure, other heterostructures have an optimum bandgap for photovoltaic applications although the PBE approximation used in this study has underestimated of electronic properties including the semiconductor bandgaps. In addition, it was found that MoSSe/WS_2 and MoSTe/WS_2 heterostructures exhibited a type-II band alignment, which is important to enhance the efficiency of photovoltaics. However, it was difficult to identify the band alignment of WSSe/WS_2 heterostructure and further calculations are necessary to realize its band alignment.

In general, this study presented a novel 2D heterostructures that are promising candidates for photovoltaic applications especially the Janus MoSSe/WS_2 heterostructures.

5.2 Future Outlook

The following points are recommended for further study:

In the present research, JTMDs/WS_2 heterostructures exhibited many interesting properties. In the future, the heterostructures can be studied using Heyd-Scuseria-Ernzerhof (HSE06) hybrid functional approximation to get better electronic structure and properties, which therefore, will significantly improve their suitability and efficiency for photovoltaic and water splitting applications

Future works can examine the optimum spacing between the two adjacent layers, the binding energies, and band energies of the heterobilayer systems with different interlayer distances to get better electronics structure and optical properties.

Further studies are also recommended to modulate the MoSTe/WS_2 bilayer heterostructure by doping other heavy elements to create stress in the structure and enhance its electronic and optical properties.

Finally, experimental works can be performed to validate the theoretical results.

References

[1] Central Statical Agence, Ethiopia, 2019.

[2] G. Coast, J. Rawlings, N. P. Par, N. Ad, D. A. O-addo, and B. Faso, “Africa :: Ghana — The World Factbook - Central Intelligence Agency Africa :: Ghana — The World Factbook - Central Intelligence Agency,”, 2020.

[3] W. Shockley and H. J. Queisser, “Detailed balance limit of efficiency of p-n junction solar cells,” *J. Appl. Phys.*, 1961.

[4] X. Li *et al.*, “Graphene-on-silicon schottky junction solar cells,” *Adv. Mater.*, 2010.

[5] J. Ortiz Balbuena, P. Tutor De Ureta, E. Rivera Ruiz, and S. Mellor Pita, “Enfermedad de Vogt-Koyanagi-Harada,” *Med. Clin. (Barc).*, 2016.

[6] D. J. Late, C. S. Rout, D. Chakravarty, and S. Ratha, “Emerging Energy Applications of Two - Dimensional Layered Materials,”, 2015.

[7] J. Wang *et al.*, “Intriguing electronic and optical properties of two-dimensional Janus transition metal,”, 2018.

[8] W. Choi, N. Choudhary, G. H. Han, J. Park, D. Akinwande, and Y. H. Lee, “Recent development of two-dimensional transition metal dichalcogenides and their applications,” *Mater. Today*, 2017.

[9] G. Oxide and M. Donarelli, “2D Materials for Gas Sensing Applications : A Review,” 2018.

[10] Q. H. Wang, K. Kalantar-Zadeh, A. Kis, J. N. Coleman, and M. S. Strano, “Electronics and optoelectronics of two-dimensional transition metal dichalcogenides,” *Nat. Nanotechnol.*, 2012.

[11] Sanjay Behura and Vikas Berry "Two-dimensional Semiconductors,” , 2015.

[12] M. Bernardi, M. Palummo, and J. C. Grossman, “Extraordinary sunlight absorption and one nanometer thick photovoltaics using two-dimensional monolayer materials,” *Nano Lett.*, 2013.

[13] G. Bin Liu, D. Xiao, Y. Yao, X. Xu, and W. Yao, “Electronic structures and theoretical modelling of two-dimensional group-VIB transition metal dichalcogenides,” *Chem. Soc. Rev.*, 2015.

[14] E. Commission, *Photovoltaic solar energy-development and current research*, 2009.

[15] S. S. Varghese, S. H. Varghese, S. Swaminathan, K. K. Singh, and V. Mittal, “Two-dimensional materials for sensing: Graphene and beyond,” *Electron.*, 2015.

[16] K. F. Mak and J. Shan, “Photonics and optoelectronics of 2D semiconductor transition metal dichalcogenides,” *Nat. Photonics*, 2016.

[17] C. H. Lee *et al.*, “Atomically thin p-n junctions with van der Waals heterointerfaces,” *Nat. Nanotechnol.*, 2014.

[18] A. K. Geim and I. V. Grigorieva, “Van der Waals heterostructures,” *Nature*, 2013.

[19] W. Wang and M. Li, “The Electronic Properties of O-Doped Pure and Sulfur Vacancy-Defect Monolayer WS 2 :”,2017

[20] J. Wang *et al.*, “Intriguing electronic and optical properties of two-dimensional Janus transition metal dichalcogenides,” *Phys. Chem. Chem. Phys.*, 2018.

[21] S. Roy and P. Bermel, “Electronic and optical properties of ultra-thin 2D tungsten disulfide for photovoltaic applications,” *Sol. Energy Mater. Sol. Cells*, 2018.

[22] H. Jiang, “Electronic band structures of molybdenum and tungsten dichalcogenides by the GW approach,” *J. Phys. Chem. C* , 2012.

[23] F. Li, W. Wei, P. Zhao, B. Huang, and Y. Dai, “Electronic and Optical Properties of Pristine and Vertical and Lateral Heterostructures of Janus MoSSe and WSSe,” *J. Phys. Chem. Lett.*, 2017.

[24] W. Liao, Y. Huang, H. Wang, and H. Zhang, “Van der Waals heterostructures for optoelectronics : Progress and prospects,” *Appl. Mater. Today*, 2019.

[25] D. Jariwala, A. R. Davoyan, J. Wong, and H. A. Atwater, “Van der Waals Materials for Atomically-Thin Photovoltaics : Promise and Outlook,” , 2017.

[26] P. Lin and J. Yang, “Tunable WSe 2 / WS 2 van der Waals heterojunction for self-powered photodetector and photovoltaics,” *J. Alloys Compd.*, 2020.

[27] P. Rivera *et al.*, “Observation of long-lived interlayer excitons in monolayer MoSe 2-WSe 2 heterostructures,” *Nat. Commun.*, 2015.

[28] K. Ren, M. Sun, Y. Luo, S. Wang, J. Yu, and W. Tang, “Applied Surface Science First-principle study of electronic and optical properties of two-dimensional materials-based heterostructures based on transition metal dichalcogenides and boron phosphide,” *Appl. Surf. Sci.*, 2019.

[29] S. Roy and P. Bermel, “Solar Energy Materials and Solar Cells Electronic and optical

properties of ultra-thin 2D tungsten disul fi de for photovoltaic applications," *Sol. Energy Mater. Sol. Cells*, 2018.

[30] B. Zhou *et al.*, "A type-II GaSe/GeS heterobilayer with strain enhanced photovoltaic properties and external electric field effects," *J. Mater. Chem. C*, 2019.

[31] Y. U. Wen *et al.*, "WS 2 /Silicon Heterojunction Solar Cells," , 2017.

[32] R. Chaurasiya, G. K. Gupta, and A. Dixit, "Solar Energy Materials and Solar Cells Ultrathin Janus WSSe bu ff er layer for W (S / Se) 2 absorber based solar cells : A hybrid , DFT and macroscopic , simulation studies," *Sol. Energy Mater. Sol. Cells*, 2019.

[33] F. Wu *et al.*, "High efficiency and fast van der Waals hetero-photodiodes with a unilateral depletion region," *Nat. Commun*, 2019.

[34] T. Jecko, "To cite this version : HAL Id : hal-00803621 On the mathematical treatment of the," 2014.

[35] C. H. Chu and C. W. Leung, "The convolution equation of Choquet and Deny on [IN]-groups," *Integr. Equations Oper. Theory*, 2001.

[36] J. P. Perdew, A. Ruzsinszky, J. Tao, V. N. Staroverov, G. E. Scuseria, and G. I. Csonka, "Prescription for the design and selection of density functional approximations: More constraint satisfaction with fewer fits," *J. Chem. Phys.*, 2005.

[37] Ashcroft mermin "Solid state physics", 1976

[38] J. D. Pack and H. J. Monkhorst, "'special points for Brillouin-zone integrations'-a reply," *Phys. Rev. B*, 1977.

[39] P. Giannozzi *et al.*, "QUANTUM ESPRESSO: A modular and open-source software project for quantum simulations of materials," *J. Phys. Condens. Matter*, 2009.

[40] J. Enkovaara, C. Rostgaard, and J. J. Mortensen, "Advanced capabilities for materials modelling with Quantum ESPRESSO.", 2017

[41] M. Zhu *et al.*, "Vasp," , 2011.

[42] M. Studio, "CASTEP Guide Materials Studio 2019," *Biovia*, 2019.

[43] R. Wolfson, "La corona solar," pp. , 2014.

[44] J. P. Perdew, K. Burke, and M. Ernzerhof, "Generalized gradient approximation made simple," *Phys. Rev. Lett.*, 1996.

[45] J. P. Perdew, K. Burke, and M. Ernzerhof, "Generalized Gradient Approximation Made Simple (vol 77, pg 3865, 1996)," *Phys. Rev. Lett.*, 1997.

[46] M. C. Payne, M. P. Teter, D. C. Allan, T. A. Arias, and J. D. Joannopoulos, “Iterative minimization techniques for ab initio total-energy calculations: Molecular dynamics and conjugate gradients,” *Rev. Mod. Phys.*, 1992.

[47] A. Allouche, “Software News and Updates Gabedit — A Graphical User Interface for Computational Chemistry Softwares,” *J. Comput. Chem.*, 2012.

[48] M. Yagmurcukardes, C. Sevik, and F. M. Peeters, “Electronic, vibrational, elastic, and piezoelectric properties of monolayer Janus MoSTe phases: A first-principles study,” *Phys. Rev. B*, 2019.

[49] X. Yang, D. Singh, Z. Xu, Z. Wang, and R. Ahuja, “An emerging Janus MoSeTe material for potential applications in optoelectronic devices,” *J. Mater. Chem. C*, 2019.

[50] W. Zhou, J. Chen, Z. Yang, J. Liu, and F. Ouyang, “Geometry and electronic structure of monolayer, bilayer, and multilayer Janus WSSe,” *Phys. Rev. B*, 2019.

[51] T. V. Vu *et al.*, “Graphene/WSeTe van der Waals heterostructure: Controllable electronic properties and Schottky barrier via interlayer coupling and electric field,” *Appl. Surf. Sci.*, 2020.

[52] M. A. U. Absor, H. Kotaka, F. Ishii, and M. Saito, “Tunable spin splitting and spin lifetime in polar WSTe monolayer,” *Jpn. J. Appl. Phys.*, 2018.

[53] M. Mohl *et al.*, “2D Tungsten Chalcogenides : Synthesis , Properties and Applications,” , 2020.

[54] A. C. N. Mos, “RSC Advances,” , 2019.

[55] S. Deng, L. Li, and P. Rees, “Graphene / MoXY Heterostructures Adjusted by Interlayer Distance , External Electric Field , and Strain for Tunable Devices,” *ACS Appl. Nano Mater.*, 2019.

[56] L. Ju, M. Bie, X. Tang, J. Shang, and L. Kou, “Energy , Environmental , and Catalysis Applications Janus WSSe Monolayer : Excellent Photocatalyst for Overall Water-splitting Janus WSSe Monolayer : Excellent Photocatalyst for Overall Water-,” 2020.

[57] V. A. Online *et al.*, “Bandgap tuning in MoSSe bilayers : synergistic effects of dipole moment and interlayer distance,” , 2018.

[58] A. Kuc, N. Zibouche, and T. Heine, “Influence of quantum confinement on the electronic structure of the transition metal sulfide T S 2,” , 2011.

[59] S. Bhattacharyya and A. K. Singh, “Semiconductor-metal transition in semiconducting

bilayer sheets of transition metal dichalcogenides,", 2012.

[60] K. D. Pham, C. V. Nguyen, H. T. T. Phung, H. V. Phuc, B. Amin, and N. N. Hieu, "Strain and electric field tunable electronic properties of type-II band alignment in van der Waals GaSe/MoSe 2 heterostructure," *Chem. Phys.*, 2019.

Appendix A: Quantum Espresso Input Files

Appendix A-I: WS2 Monolayer SCF Calculation Input Files

Input files below that enabled us to calculate the total energy, total force, bandgap, density of state and others. These input files contain important information about the system.

```
&control
Calculation = 'scf':
   restart_mode='from_scratch',
   prefix='ws2',
tstress =. true.
tprnfor =. true.
   pseudo_dir = './',
   outdir='./'
   verbosity='high',
forc_conv_thr = 0.01D-3
etot_conv_thr = 1D-6
/
```

From &control to / are grouped together, and between them parameters are set in the format of "parameter name = value". The "calculation" parameter specifies the calculation mode. Here it is 'scf'. This means self-consistent calculation (solving the Kohn-Sham equation self-consistently). The "prefix" parameter specifies the header for output files. It is a good idea to specify a material name. Here, it is 'ws2'. The "pseudo_dir" parameter is the location of the pseudopotential file. Now the pseudopotential files are located in the same working directory, so for now we'll use './' (meaning the present working directory). 'from_scratch': This is the normal way to perform a PWscf calculation. tstress =. true. To calculate stress. tprnfor =. true. To calculate force. verbosity to "high" in quantum espresso. In that case it will print out all the eigenvalues.

etot_conv_thr: Convergence threshold on total energy (a.u) for ionic minimization: the convergence criterion is satisfied when the total energy changes less than etot_conv_thr between two consecutive scf steps.forc_conv_thr: Convergence threshold on forces (a.u) for ionic minimization the convergence criterion is satisfied when all components of all forces are smaller than forc_conv_thr.

```
&SYSTEM
  ibrav = 4
  a =    3.18
  c =    18.323
  nat = 3
  ntyp = 2
  ecutwfc=60,
  ecutrho=600,
```

```
  input_dft='pbe',
  occupations='smearing',
  degauss     = 0.05
  smearing = 'gaussian'
  vdw_corr='grimme-d2
/
```

This paragraph is a part that expresses the characteristics of the system. “ibrav” is a way to specify the Bravais lattice, and “ibrav = 4” specifies the unit cell vector of hexagonal. WS2 has the hexagonal crystal structure. Let’s watch out. “a” and “c” represents the lattice constant, “nat” represents the number of atoms in the unit cell, and “ntyp” represents the number of elements. “ecutwfc” and “ecutrho” are the cutoff energies (unit is Rydberg). Increasing the cutoff value, increases the accuracy, but makes the calculation heavier. The recommended value depends on the type of pseudopotential and from the convergence test from chapter five.

```
&ELECTRONS
 mixing_mode = 'plain'
 conv_thr=1d-08
 mixing_beta=0.7
/
```

This paragraph specifies the parameters for the convergence of the wave function. “conv_thr” is a parameter used for convergence judgment. “mixing_mode” and “mixing_beta” are parameters to speed up convergence.

```
ATOMIC_SPECIES
S 32.06750 S.pbe-n-kjpaw_psl.1.0.0.UPF
W 183.84000 W.pbe-spn-kjpaw_psl.1.0.0.UPF
```

This part specifies the atom type and atomic weight and the pseudopotential file. As already mentioned in chapter three, pseudopotentials can be downloaded from the page in Quantum ESPRESSO.

```
ATOMIC_POSITIONS {crystal}
W   0.000000000000000   0.000000000000000   0.500000000000000
S   0.666666666666667   0.333333333333333   0.586677000000000
S   0.666666666666667   0.333333333333333   0.413323000000000
```

This represents the internal coordinates (xyz coordinates) in the W and two S unit cells.

```
K_POINTS {automatic}
  12 12 1 0 0 0
```

The last part specifies the number of points (k points) in the wavenumber vector. The first three numbers specify the number of wavenumber divisions in the x, y, and z directions. {Automatic} is specified, k points are automatically taken discretely in the first Brillouin zone. The last three

numbers describe the wave number origin shift. Here, there is no shift (all 0). The more k points the more accurate the calculation, but the slower the calculation. In the self-consistent calculation, it takes time to repeat the calculation until the electron density converges, so the number of k points is taken from the convergence test from chapter five.